Energy Conversion and Management 171 (2018) 1822–1842

Contents lists available at ScienceDirect

Energy Conversion and Management

journal homepage: www.elsevier.com/locate/enconman

Performance comparison of exponential, Lambert *W* function and Special Trans function based single diode solar cell models

Xiankun Gao[a], Yan Cui[a,*], Jianjun Hu[a], Nadeem Tahir[a,b], Guangyin Xu[a]

[a] Key Laboratory of New Materials and Facilities for Rural Renewable Energy, Ministry of Agriculture, Henan Agricultural University, Zhengzhou 450002, China
[b] Collaborative Innovation Center of Biomass Energy, Henan Agricultural University, Zhengzhou 450002, China

ARTICLE INFO

Keywords:
Solar cell
Single diode model
Lambert *W* function
Special Trans function
Parameter extraction

ABSTRACT

Accurate modeling plays an important role in solar cell simulation. In order to reveal the applicability and superiority of Special Trans function based single diode model (SBSDM), this paper presents a comprehensive comparison of SBSDM, Lambert *W* function based single diode model (LBSDM) and exponential-type single diode model (SDM). The performance difference of SBSDM, LBSDM and SDM is verified and compared in two aspects: (1) different fitness to the measured *I–V* data of solar cells and (2) different parameter extraction performance. To be objective and reproducible, the reported parameter values of standard datasets and measured datasets are employed to validate the fitness difference of the three models. The comparison results indicate that SBSDM always exhibits better fitness than LBSDM and SDM in representing the *I–V* characteristics of various solar cells and can provide a closer prediction to actual maximum power points. With the help of a ranking based branch selection strategy, a modified Nelder-Mead simplex (MNMS) algorithm is proposed to test the parameter extraction performance of SBSDM, LBSDM and SDM. The comparison results reveal that the time computational efficiency of SBSDM is inferior to SDM but superior to LBSDM. SBSDM always achieves superior accuracy and convergence speed than LBSDM and SDM, although lacking enough statistical robustness. Due to these superiorities, SBSDM is quite promising and envisaged to be the most valuable model for solar cell parameter extraction and PV system simulation.

1. Introduction

As a promising renewable energy technology, solar cell has been extensively investigated due to its unique advantage and great potential to meet the increasing energy demands. Along with the evolution of PV technology, accurate modeling and parameter extraction for closely representing the nonlinear *I–V* (current vs. voltage) characteristics have attracted considerable attention in performance evaluation of solar cell and maximum energy harvesting of PV systems [1–4].

1.1. Brief overview of three models

Over the past years, various models have been developed to describe the electrical behavior of solar cells. In practice, the exponential-type single diode model (SDM) is undoubtedly the most widely used model due to its good compromise between simplicity and accuracy [3–7].

In the equivalent circuit of SDM illustrated in Fig. 1, the *I–V* relationship of a solar cell under illumination can be formulated by the following SDM Eq. (1).

$$I = I_{ph} - I_0\left[\exp\left(\frac{V + IR_s}{nV_{th}}\right) - 1\right] - \frac{V + IR_s}{R_{sh}} \quad (1)$$

where I, V, I_{ph}, I_0, n, R_s and R_{sh} are the terminal current, terminal voltage, photocurrent, diode saturation current, diode ideality factor, series and shunt resistances respectively. Thermal voltage $V_{th} = N_s kT/q$, where N_s is the number of cells in series, $k = 1.3806503 \times 10^{-23}$ J/K is the Boltzmann constant, $q = 1.60217646 \times 10^{-19}$ C is the electronic charge, and T is the absolute temperature in Kelvin which can be calculated by 273.15 plus the cell temperature in Celsius.

It is easy to see from Eq. (1) that there are five parameters (I_{ph}, I_0, n, R_s and R_{sh}) in SDM to be extracted as accurately as possible. These parameters are not only of vital importance for performance evaluation and quality control of solar cell, but also play a significant role in maximum power point (MPP) tracking of PV systems [7–10]. For instance, the diode ideality factor n is a real quality index indicating how closely a real solar cell follows the ideal cell, and its value depends critically upon semiconductor material and fabrication process. Thus, it

* Corresponding author.
E-mail addresses: gaoxiankun78@163.com (X. Gao), cuiyan6198@163.com (Y. Cui).

https://doi.org/10.1016/j.enconman.2018.06.106
Received 23 April 2018; Received in revised form 21 June 2018; Accepted 28 June 2018
Available online 09 July 2018
0196-8904/

Nomenclature

ACE_{cal}	absolute current error of calculated current (A)
ACE_{sim}	absolute current error of simulated current (A)
c	centroid of simplex
D	problem dimension
f_M	error function of model
F	objective function value
F_0	objective function value at start point
I	terminal current (A)
I_0	diode saturation currents (A)
I_{cal}	calculated current (A)
I_D	diode currents (A)
I_{ph}	photocurrent (A)
I_{sim}	simulated current (A)
k	Boltzmann constant ($1.3806503 \times 10^{-23}$ J/K)
LB	lower bound
LBSDM	Lambert W function based SDM
m	factorial series of STF
MaxNFEs	maximum number of function evaluations
MNMS	modified Nelder-Mead simplex
MPP	maximum power point
n	diode ideality factor
N	number of measured I–V data
N_s	number of cells in series
N_p	number of uniform sampling points
N_r	allowed number of iterations
$NFEs$	number of function evaluations
NFE_{th}	number of function evaluations at thV
NMS	Nelder-Mead simplex
P	population of N_p sample points
q	electronic charge ($1.60217646 \times 10^{-19}$ C)
R_s	series resistance (Ω)
R_{sh}	shunt resistance (Ω)
$RMSEcal$	calculated root mean square error
$RMSEsim$	simulated root mean square error
S	bound-constrained simplex
S_e	bound-constrained expansion point
S_{ic}	bound-constrained inside contraction point
S_r	bound-constrained reflection point
S_{oc}	bound-constrained outside contraction point
S_u	unconstrained simplex
S_{ue}	unconstrained expansion point
S_{uic}	unconstrained inside contraction point
S_{uoc}	unconstrained outside contraction point
S_{ur}	unconstrained reflection point
$SBSDM$	Special Trans function based SDM
SDM	single diode model
STF	Special Trans function
thV	threshold value of $RMSE_{cal}$
$trans+$	symbol of Special Trans function
T	cell temperature (K)
UB	upper bound
V	terminal voltage (V)
V_{th}	thermal voltage (V)
wc	weighted centroid
W_0	principal branch of Lambert W function
x	STF branch
x_0	initial STF branch
X	unknown parameter vector
X_0	start point
X_{u0}	unconstrained surrogate of X_0
α	reflection coefficient
β	expansion coefficient
γ	contraction coefficient
δ	shrinkage coefficient

is essential to extract these parameters accurately from the measured I–V data of solar cells. Unfortunately, SDM Eq. (1) is an implicit transcendental equation and has the shortcoming of being explicitly unsolvable for either current I or voltage V only using common elementary functions [11]. This inherently implicit nature hampers not only solar cell parameter extraction [12] but also PV system simulation [2].

In order to circumvent this difficulty, some researchers have diverted their attention to the mathematical improvement of SDM Eq. (1). Authors in [13] reported a Lambert W function [14] based single diode model (LBSDM) Eq. (2).

$$I = \frac{R_{sh}(I_{ph} + I_0) - V}{R_s + R_{sh}} - \frac{nV_{th}}{R_s} W_0(U) \tag{2}$$

where W_0 is the principal branch of Lambert W function, and

$$U = \frac{I_0 R_s R_{sh}}{nV_{th}(R_s + R_{sh})} \exp\left[\frac{R_{sh}(R_s I_{ph} + R_s I_0 + V)}{nV_{th}(R_s + R_{sh})}\right] \tag{3}$$

Clearly, LBSDM Eq. (2) is an exact explicit expression of implicit

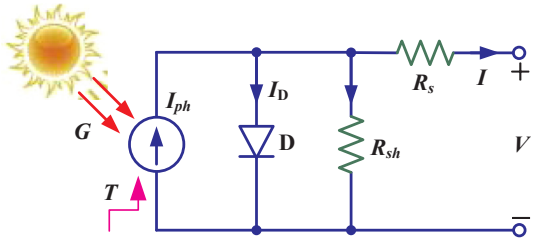

Fig. 1. The single diode model of a solar cell under illumination.

SDM Eq. (1). The application of LBSDM Eq. (2) have been summarized in one of our previous papers [15]. To sum up, LBSDM Eq. (2) has better accuracy and convergence than SDM Eq. (1). Regrettably, since the computational speed of Lambert W function is 2.8–4.1 times slower than that of exponential function [16], LBSDM Eq. (2) is computationally more expensive and time consuming than SDM Eq. (1) [17].

As an alternative to Lambert W function, the Special Trans function (STF) defined in [18] has been proved to be superior within Maple and Mathematica environment. This enables many transcendental equations involving exponential terms can be solved using STF. In particular, STF has been successfully applied to obtain the exact explicit expression of SDM Eq. (1). After some structural modifications, the STF based single diode model (SBSDM) reported in [19–23] can be rewritten as Eq. (4).

$$I = \frac{R_{sh}(I_{ph} + I_0) - V}{R_s + R_{sh}} - \frac{nV_{th}}{R_s} trans_+(x, U) \tag{4}$$

where $trans_+(x, U)$ is the STF defined as

$$trans_+(x, U) = U \frac{\sum_{m=0}^{[x]} U^m (x-m)^m / m!}{\sum_{m=0}^{[x+1]} U^m (x+1-m)^m / m!} \tag{5}$$

where $[x]$ denotes the greatest integer less than or equal to x. Since the number of accurate digits in the numerical structure of $trans_+(x, U)$ depends upon $[x]$ and for practical analysis [18], $trans_+(x, U)$ can be treated as a multi-branch function of $x \subset \mathbb{Z}^+$. Due to the factorial of m is only accurate for $m \leq 21$ in commonly used double-precision arithmetic, in this paper the STF branch x is assigned to be a positive integer less than or equal to 20, i.e. $x \in \{1, 2, \ldots, 20\} \subset \mathbb{Z}^+$.

The common feature of LBSDM Eq. (2) and SBSDM Eq. (4) is that for any value of voltage V, the corresponding exact value of current I can be

calculated straightforwardly. On the other hand, the only difference between them lies in the definition of Lambert *W* function and STF. Since the concept of STF is fundamentally different from Lambert *W* function, SBSDM Eq. (4) should yield impressive results for parameter extraction of solar cells.

1.2. Current problems of SBSDM in solar cell simulation

An exhaustive examination of the literatures indicates there is less work on the application of SBSDM Eq. (4) in solar cell simulation. Existing works mainly focused on substituting some known parameter values into SBSDM Eq. (4) to calculate the diode ideality factor [19–21], the optimum load [22], several key points on *I–V* curve such as short-circuit current, open-circuit voltage, MPP and curve slopes at axis intersections [23]. STF, of course, has also been used to yield the exact explicit expression for organic solar cells showing *S*-shaped *I–V* characteristics [24]. Nevertheless, it is regrettable that the existing works manifest the accuracy of SBSDM Eq. (4) within Maple and Mathematica environment using more than 20 digit precision [21,23]. It remains to be seen whether this accuracy still holds true in commonly used double precision arithmetic. Moreover, existing works were generally confined in the scope of one-dimensional parameter extraction using analytical method; none of them involves utilizing numerical algorithm to extract all model parameters of SBSDM Eq. (4) form the measured *I–V* data of solar cells. Furthermore, since existing works only consider the several key points on *I–V* curve, there still lacks a comprehensive evaluation to examine whether SBSDM Eq. (4) could better fit all measured *I–V* data under the same conditions.

1.3. Main contributions of this work

In light of above issues, the main objective of this work is to make a

Table 1
$RMSE_{cal}$ values of SDM, LBSDM and SBSDM calculated using the measured *I–V* data of R.T.C. France solar cell [28] and the parameter values extracted by various algorithms. The optimal *x* for computing the minimum $RMSE_{cal}$ value of SBSDM is also listed hereinafter.

No.	Algorithm	Parameters					$RMSE_{cal}$			
		I_{ph} (A)	I_0 (μA)	n	R_s (Ω)	R_{sh} (Ω)	SDM	LBSDM	SBSDM	Optimal x
1	EHA-NMS [5]	0.760776	0.323021	1.481184	0.036377	53.718521	9.8602E−04	7.7539E−04	7.7527E−04	7
2	R_{cr}-IJADE [29]	0.760776	0.323021	1.481184	0.036377	53.718526	9.8602E−04	7.7539E−04	7.7527E−04	7
3	ER-WCA [30]	0.760776	0.322699	1.481080	0.036381	53.69100	9.8609E−04	7.7529E−04	7.7518E−04	7
4	CSO [31]	0.76078	0.3230	1.48118	0.03638	53.7185	9.8612E−04	7.7544E−04	7.7531E−04	7
5	NM-MPSO [32]	0.76078	0.32306	1.48120	0.03638	53.7222	9.8620E−04	7.7550E−04	7.7536E−04	6
6	BMO [33]	0.76077	0.32479	1.48173	0.03636	53.8716	9.8622E−04	7.7621E−04	7.7610E−04	7
7	LMSA [34]	0.76078	0.31849	1.47976	0.03643	53.32644	9.8649E−04	7.7406E−04	7.7394E−04	7
8	BBO-M [35]	0.76078	0.31874	1.47984	0.03642	53.36227	9.8656E−04	7.7423E−04	7.7412E−04	7
9	GOTLBO [36]	0.760780	0.331552	1.483820	0.036265	54.115426	9.8744E−04	7.7979E−04	7.7969E−04	7
10	IADE [26]	0.7607	0.33613	1.4852	0.03621	54.7643	9.9076E−04	7.8442E−04	7.8434E−04	7
11	GGHS [37]	0.76092	0.32620	1.48217	0.03631	53.0647	9.9089E−04	7.8146E−04	7.8137E−04	7
12	ABSO [38]	0.76080	0.30623	1.47583	0.03659	52.2903	9.9125E−04	7.7368E−04	7.7352E−04	7
13	CS [39]	0.7608	0.323	1.4812	0.0364	53.7185	9.9161E−04	7.7779E−04	7.7725E−04	6
14	PPSO [40]	0.7608	0.3230	1.4812	0.0364	53.7185	9.9161E−04	7.7779E−04	7.7725E−04	6
15	HS [37]	0.76070	0.30495	1.47538	0.03663	53.5946	9.9515E−04	7.7625E−04	7.7609E−04	7
16	STLBO [41]	0.76078	0.32302	1.48114	0.03638	53.7187	9.9763E−04	7.8059E−04	7.7567E−04	4
17	TLBO [41]	0.76074	0.32378	1.48136	0.03641	54.4029	1.0016E−03	7.8421E−04	7.8047E−04	4
18	DE [35]	0.76068	0.35515	1.49080	0.03598	56.5533	1.0035E−03	8.0173E−04	8.0167E−04	7
19	IGHS [37]	0.76077	0.34351	1.48740	0.03613	53.2845	1.0335E−03	8.2116E−04	8.1409E−04	4
20	MSSO [11]	0.760777	0.323564	1.481244	0.036370	53.742465	1.0599E−03	8.0916E−04	7.8338E−04	4
21	PCE [42]	0.760776	0.323021	1.481074	0.036377	53.718525	1.0606E−03	8.0924E−04	7.8330E−04	4
22	ABC [43]	0.7608	0.3251	1.4817	0.0364	53.6433	1.0967E−03	8.3343E−04	8.0510E−04	4
23	HPEPD [44]	0.7607884	0.3102482	1.4769641	0.03655304	52.859056	1.1487E−03	8.4728E−04	8.0663E−04	4
24	FPA [45]	0.76079	0.310677	1.47707	0.0365466	52.8771	1.2121E−03	8.7797E−04	8.2890E−04	4
25	BPFPA [46]	0.7600	0.3106	1.4774	0.0366	57.7151	1.2536E−03	9.5551E−04	9.5306E−04	6
26	LI [47]	0.7609438	0.3456572	1.48799169	0.03614233	49.482205	1.3462E−03	1.0548E−03	1.0223E−03	4
27	CPSO [48]	0.7607	0.4000	1.5033	0.0354	59.012	1.3861E−03	1.0255E−03	1.0237E−03	6
28	MPCOA [49]	0.76073	0.32655	1.48168	0.03635	54.6328	2.3131E−03	1.4692E−03	1.3708E−03	4
29	DE [50]	0.76077	0.32302	1.48059	0.03637	53.7185	2.3423E−03	1.4810E−03	1.3813E−03	4
30	TMP [51]	0.7610	0.3635	1.4935	0.03660	62.574	2.3859E−03	1.5051E−03	1.0505E−03	3
31	BBO [35]	0.76098	0.86100	1.58742	0.03214	78.8555	2.3929E−03	2.0021E−03	2.0018E−03	6
32	MABC [52]	0.760779	0.321323	1.481385	0.036389	53.39999	2.7610E−03	1.7277E−03	1.2892E−03	2
33	ABCDE [50]	0.76077	0.32302	1.47986	0.03637	53.7185	4.8548E−03	2.9246E−03	2.8098E−03	4
34	TLBO [53]	0.760809	0.312244	1.47578	0.036551	52.8405	7.2723E−03	4.3349E−03	4.2169E−03	4
35	GWO [53]	0.760996	0.2430388	1.451219	0.037732	45.116309	7.2845E−03	4.3496E−03	4.2360E−03	4
36	TVACPSO [53]	0.760788	0.3106827	1.475258	0.036547	52.889644	7.3438E−03	4.3680E−03	4.2494E−03	4
37	WCA [53]	0.760908	0.4135540	1.504381	0.035363	57.669488	7.6069E−03	4.6472E−03	4.5362E−03	4
38	CARO [54]	0.76079	0.31724	1.48168	0.03644	53.0893	8.1969E−03	4.9502E−03	3.0376E−03	2
39	PSO [55]	0.760798	0.322721	1.48382	0.0363940	53.7965	9.6545E−03	5.8310E−03	3.8563E−03	2
40	TLBO [56]	0.7608	0.3223	1.4837	0.0364	53.76027	9.6960E−03	5.8554E−03	3.8808E−03	2
41	Newton [28]	0.7608	0.3223	1.4837	0.0364	53.76344	9.6964E−03	5.8556E−03	3.8810E−03	2
42	ABSO [50]	0.76080	0.30623	1.47986	0.03659	52.2903	1.4169E−02	8.5524E−03	6.5442E−03	2
43	PS [57]	0.7617	0.9980	1.6000	0.0313	64.10256	1.4936E−02	9.8170E−03	9.7428E−03	4
44	SA [58]	0.7620	0.4798	1.5172	0.0345	43.10345	1.8998E−02	1.1655E−02	1.1545E−02	4
45	GA [59]	0.7619	0.8087	1.5751	0.0299	42.37288	1.9078E−02	1.2009E−02	1.1929E−02	4
46	DET [60]	0.751	0.315	1.487	0.036	54.532	2.4481E−02	1.5845E−02	1.3918E−02	2
47	MPSO [50]	0.76077	0.32302	1.47086	0.03637	53.7185	3.9022E−02	2.2470E−02	2.2341E−02	4
48	ICA [61]	0.7603	0.14650	1.4421	0.0389	41.1577	1.1582E−01	7.5021E−02	7.3189E−02	2
49	MBA [62]	0.7604	0.2348	1.4890	0.0388	44.61	1.1672E−01	7.6204E−02	7.4341E−02	2
50	MVO [63]	0.7616	0.32094	1.5252	0.0365	59.5884	1.2680E−01	8.6278E−02	8.4561E−02	2

comprehensive performance comparison of SBSDM, LBSDM and SDM thereby revealing the applicability and superiority of SBSDM. The first contribution of this paper is to verify their respective fitness to the measured *I–V* data of various solar cells. The fitness comparison is designed to find out which of them can better represent the measured *I–V* characteristics of solar cells under the same parameter values. For objectivity and reproducibility, the fitness comparison is carried out using the reported parameter values of standard datasets and measured datasets of four solar cell/modules. The second contribution of this paper is to compare the parameter extraction performance of SDM, LBSDM and SBSDM using numerical algorithm, so as to reveal which of them can extract more accurate parameter values under same simulation conditions. To this end, a ranking based branch selection strategy and a modified Nelder-Mead simplex (MNMS) algorithm are proposed for parameter extraction of the three models. The accuracy, convergence speed, computation time and robustness of the three models are compared in detail. To the best of our knowledge, this is the first numerical parameter extraction of SBSDM and thus deserves serious attention.

The rest of this paper is organized as follows. Section 2 focuses on the fitness comparison of SBSDM, LBSDM and SDM. Section 3 introduces the objective function used in parameter extraction. Section 4 presents the MNMS algorithm and the ranking based STF branch selection strategy. Section 5 elaborates and compares the parameter extraction results, and finally, Section 6 concludes this paper and provides some directions for future research.

2. Fitness comparison of SBSDM, LBSDM and SDM

On the surface, LBSDM Eq. (2) and SBSDM Eq. (4) are exactly derived from SDM Eq. (1) with the identical model parameters, so they should have the same performance. In fact, they are closely linked with but different from each other. Owing to the difference of exponential function, Lambert *W* function and STF, they are expressed and calculated in different ways, and thus have different fitness to the measured *I–V* data of solar cells.

2.1. Fitness criterion

A fitness criterion should be defined prior to quantifying and comparing the fitness of SDM, LBSDM and SBSDM under the same conditions. Substituting the measured *I–V* data, the parameter values of I_{ph}, I_0, n, R_s, R_{sh} and the STF branch x into the right side of Eqs. (1), (2) and (4), the calculated currents of the three models can be represented respectively by

$$I_{cal\_SDM} = I_{ph} - I_0\left[\exp\left(\frac{V + IR_s}{nV_{th}}\right) - 1\right] - \frac{V + IR_s}{R_{sh}} \tag{6}$$

$$I_{cal\_LBSDM} = \frac{R_{sh}(I_{ph} + I_0) - V}{R_s + R_{sh}} - \frac{nV_{th}}{R_s}W_0(U) \tag{7}$$

$$I_{cal\_SBSDM} = \frac{R_{sh}(I_{ph} + I_0) - V}{R_s + R_{sh}} - \frac{nV_{th}}{R_s}trans_+(x, U) \tag{8}$$

Consequently, the absolute current errors (ACE) between the measured current and the calculated current of above three models can be generally expressed as

$$ACE_{cal} = |I - I_{cal}| \tag{9}$$

Similar to the fitness function defined in [25–27], the root mean square error (RMSE) between the measured current and calculated current is chosen as the criterion to quantify the fitness of SDM, LBSDM and SBSDM. For N pair of measured *I–V* data, the fitness can be generally formulated as

$$\mathrm{RMSE}_{cal} = \sqrt{\frac{1}{N}\sum_{i=1}^{N}(I - I_{cal})^2} \tag{10}$$

Table 2
RMSE_{cal} values of SDM, LBSDM and SBSDM calculated using the measured *I–V* data of Photowatt-PWP201 module [28] and the parameter values extracted by various algorithms.

No.	Algorithm	Parameters					RMSE_{cal}			
		I_{ph} (A)	I_0 (μA)	n	R_s (Ω)	R_{sh} (Ω)	SDM	LBSDM	SBSDM	Optimal x
1	EHA-NMS [5]	1.030514	3.482263	48.642835	1.201271	981.982256	2.4251E−03	2.1385E−03	2.1132E−03	4
2	R_{cr}-IJADE [29]	1.030514	3.482263	48.642835	1.201271	981.98224	2.4251E−03	2.1385E−03	2.1132E−03	4
3	PPSO [40]	1.0305	3.4823	48.6432	1.2013	981.9823	2.4254E−03	2.1389E−03	2.1133E−03	4
4	ER-WCA [30]	1.03064	3.61455	48.7890	1.19627	961.053	2.4379E−03	2.1769E−03	2.1557E−03	4
5	NM-MPSO [32]	1.0305	3.6817	48.8598	1.1944	983.9970	2.4403E−03	2.1872E−03	2.1673E−03	4
6	IADE [26]	1.0320	3.886	49.068	1.189	921.850	2.5531E−03	2.3119E−03	2.2916E−03	4
7	HPEPA [44]	1.032173	3.035367	48.123090	1.218407	783.516	2.5838E−03	2.1627E−03	2.1102E−03	4
8	HPEPB [44]	1.033537	2.825571	47.859350	1.224053	689.321	2.6429E−03	2.2105E−03	2.1585E−03	4
9	FPA [45]	1.032091	3.047538	48.13128	1.217583	811.3721	2.7425E−03	2.1994E−03	2.1657E−03	4
10	HPEPD [44]	1.0323759	2.5188848	47.426408	1.2390187	745.6431	2.7426E−03	2.1082E−03	2.0594E−03	4
11	HPEPC [44]	1.0323759	2.5188885	47.4264129	1.2390187	745.6443	2.7426E−03	2.1082E−03	2.0594E−03	4
12	LI [47]	1.0334262	2.4424001	47.32669503	1.2307473	603.4037	3.1348E−03	2.5241E−03	2.5003E−03	5
13	MPCOA [49]	1.03188	3.37370	48.50646	1.20295	849.6927	3.7823E−03	2.6345E−03	2.5302E−03	5
14	CARO [54]	1.03185	3.28401	48.40363	1.20556	841.3213	3.7831E−03	2.6128E−03	2.5052E−03	5
15	ABCDE [50]	1.0318	3.2774	48.3948	1.2062	845.2495	3.8855E−03	2.6526E−03	2.5409E−03	5
16	SA [58]	1.0331	3.6642	48.8211	1.1989	833.3333	4.1693E−03	2.9664E−03	2.8757E−03	5
17	CPSO [48]	1.0286	8.301	52.243	1.0755	1850.1	4.2128E−03	3.5222E−03	3.5061E−03	5
18	PS [57]	1.0313	3.1756	48.2889	1.2053	714.2857	4.5075E−03	3.2996E−03	3.2077E−03	5
19	GA [59]	1.0441	3.4360	48.5862	1.1968	555.5556	6.0378E−03	5.8023E−03	5.7939E−03	5
20	Newton [28]	1.0318	3.2876	48.45	1.2057	549.4505	6.5503E−03	5.5670E−03	5.5338E−03	4
21	TLBO [56]	1.031805	3.280945	48.44228	1.206	548.666	6.5671E−03	5.5789E−03	5.5457E−03	4
22	TMP [51]	1.0333	2.3326	47.1816	1.2744	715.824	6.8931E−03	3.5169E−03	3.0702E−03	4
23	ICA [53]	1.034601	2.366382	47.173884	1.238841	602.127603	7.0259E−03	4.0148E−03	3.8008E−03	5
24	TVACPSO [53]	1.031435	2.638610	47.556652	1.235611	821.595146	7.0904E−03	3.9882E−03	3.7780E−03	5
25	WCA [53]	1.031434	2.638077	47.555893	1.235634	821.641324	7.0918E−03	3.9887E−03	3.7784E−03	5
26	GWO [53]	1.033447	2.778340	47.746469	1.227743	746.622792	7.4697E−03	4.2172E−03	4.0053E−03	5
27	TLBO [53]	1.031199	2.814058	47.79082	1.226948	863.1939	7.4996E−03	4.1849E−03	3.9681E−03	5
28	ABSO [60]	1.03166	3.3731	48.5832	1.20134	852.463	8.8849E−03	5.0656E−03	4.1346E−03	3
29	DET [60]	1.03045	3.31089	48.4379	1.1063	815.647	1.2123E−02	7.2878E−03	6.1141E−03	2
30	MVO [63]	1.0324	2.5401	47.6244	1.2422	745.0	2.4881E−02	1.3062E−02	8.8430E−03	3

Under the same parameter values of I_{ph}, I_0, n, R_s and R_{sh}, it is obviously that the smaller the $RMSE_{cal}$, the better the fitness of the model to the measured I–V data of solar cells.

2.2. Fitness comparison results

To be objective and reproducible, the reported parameter values of two standard datasets and two practical measured datasets are selected and substituted into Eqs. (6)–(10) to verify the fitness difference of SDM, LBSDM and SBSDM.

2.2.1. Results on standard datasets

The two standard datasets are adopted from [28], where the measurements are carried out on a 57 mm diameter commercial silicon (R.T.C. France) solar cell operating at 33 °C and a solar module (Photowatt-PWP201) composed of 36 polycrystalline silicon cells in series operating at 45 °C. These two sets of measured I–V data are very representative, because they have been extensively adopted in literature as the benchmarks to test and compare the performance of various algorithms for parameter extraction of SDM, as shown by the algorithm acronyms and parameter values listed in Tables 1 and 2.

As mentioned in previous section, the $trans_+(x, U)$ in Eq. (5) can be treated as a multi-branch function of $x \in \{1, 2, \ldots, 20\} \subset \mathbb{Z}^+$. Hence, for each set of parameter values there is an optimal x corresponding to the minimum $RMSE_{cal}$ value of SBSDM, as shown by the marker * in Figs. 2 and 3(a). These results suggest that the parameter values are sensitive to STF branch x. However, it is not true that the bigger x the lower $RMSE_{cal}$ value of SBSDM and vice versa. Although there is no fixed rule to build the mapping relations between parameter values and STF branch x, but the optimal x is generally less than or equal to 7. The last columns of Tables 1 and 2 summarize the minimum $RMSE_{cal}$ values of SBSDM, LBSDM and SDM. For easy comparison and crosschecking, they are plotted in Figs. 2 and 3(b). It is clear that all $RMSE_{cal}$ values of SDM are remarkably larger than that of LBSDM, while all $RMSE_{cal}$ values of LBSDM are slightly bigger than that of SBSDM. This indicates that SBSDM has better fitness to standard datasets as compared to LBSDM and SDM. To illustrate this, Figs. 2 and 3(c) plot the measured current and calculated currents versus voltage. A close inspection of Figs. 2 and 3(c) reveals that the calculated currents of SBSDM, LBSDM and SDM have different agreements with the measured current. To better circumstantiate these disagreements, Figs. 2 and 3(d) put into evidence the absolute current errors. It is evident that the absolute current errors of SBSDM are smaller comparing with those of LBSDM and SDM, especially in the region of high voltage. This confirms that SBSDM can better fit standard datasets under the same parameter values of I_{ph}, I_0, n, R_s and R_{sh}. It is worth mentioning that the difference of absolute current errors of SBSDM, LBSDM and SDM depends strongly upon the accuracy of the parameter values listed in Tables 1 and 2. In general, the more accurate the parameter values are, the less the difference of absolute current errors. Furthermore, from the zoomed-in views of Figs. 2 and 3(d), one can see that although there is negligible difference between SBSDM and LBSDM, but around MPP SBSDM exhibits smaller absolute current errors in comparison with LBSDM and SDM. This means that SBSDM has lesser absolute power errors and can provide a closer representation to the actual MPP of standard datasets.

2.2.2. Results on measured datasets

The two measured datasets are gotten from [51], where a simple

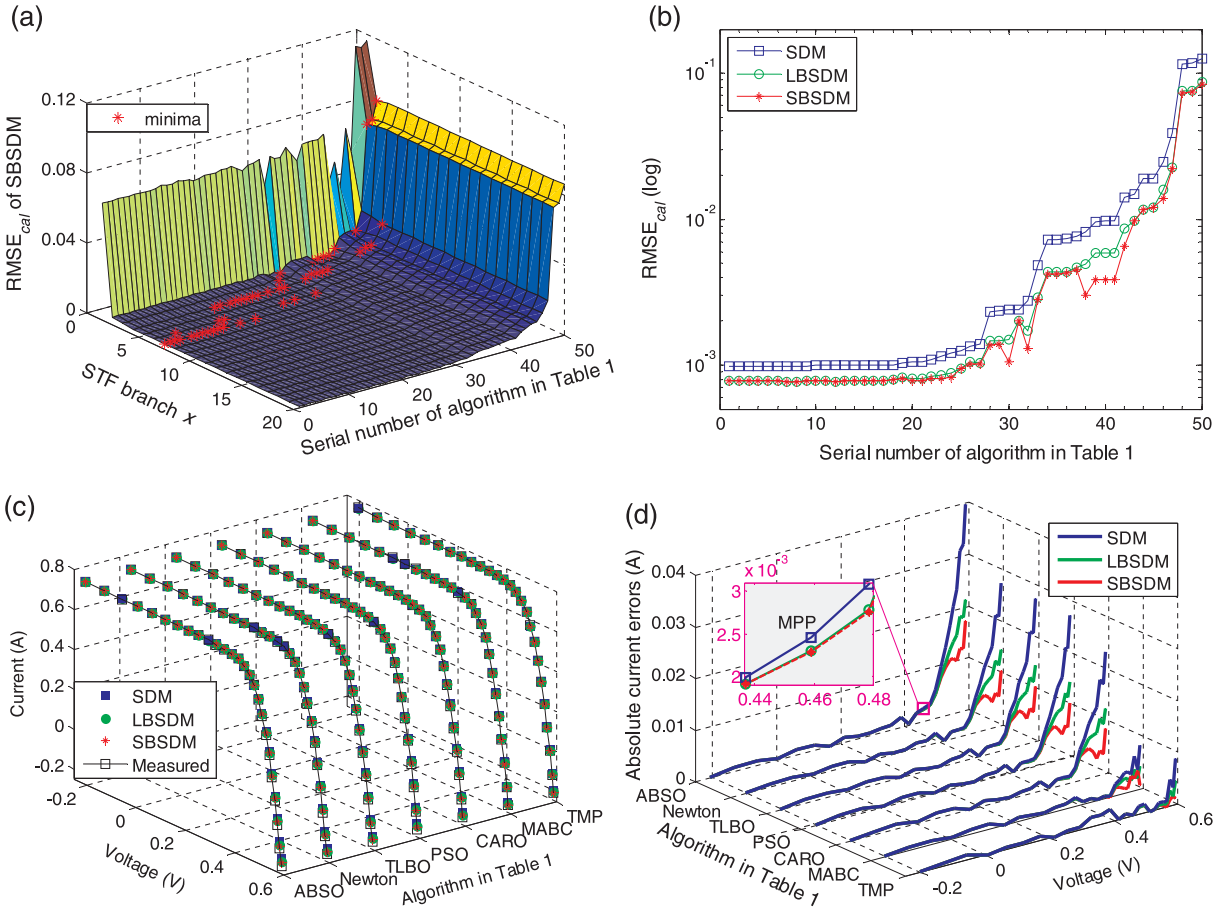

Fig. 2. Calculated curves of SDM, LBSDM and SBSDM using the measured I–V data of R.T.C France solar cell [28] and the parameter values extracted by various algorithms in Table 1: (a) $RMSE_{cal}$ values of SBSDM at different STF branch x, (b) comparison of $RMSE_{cal}$ values, (c) I–V characteristics and (d) absolute current errors.

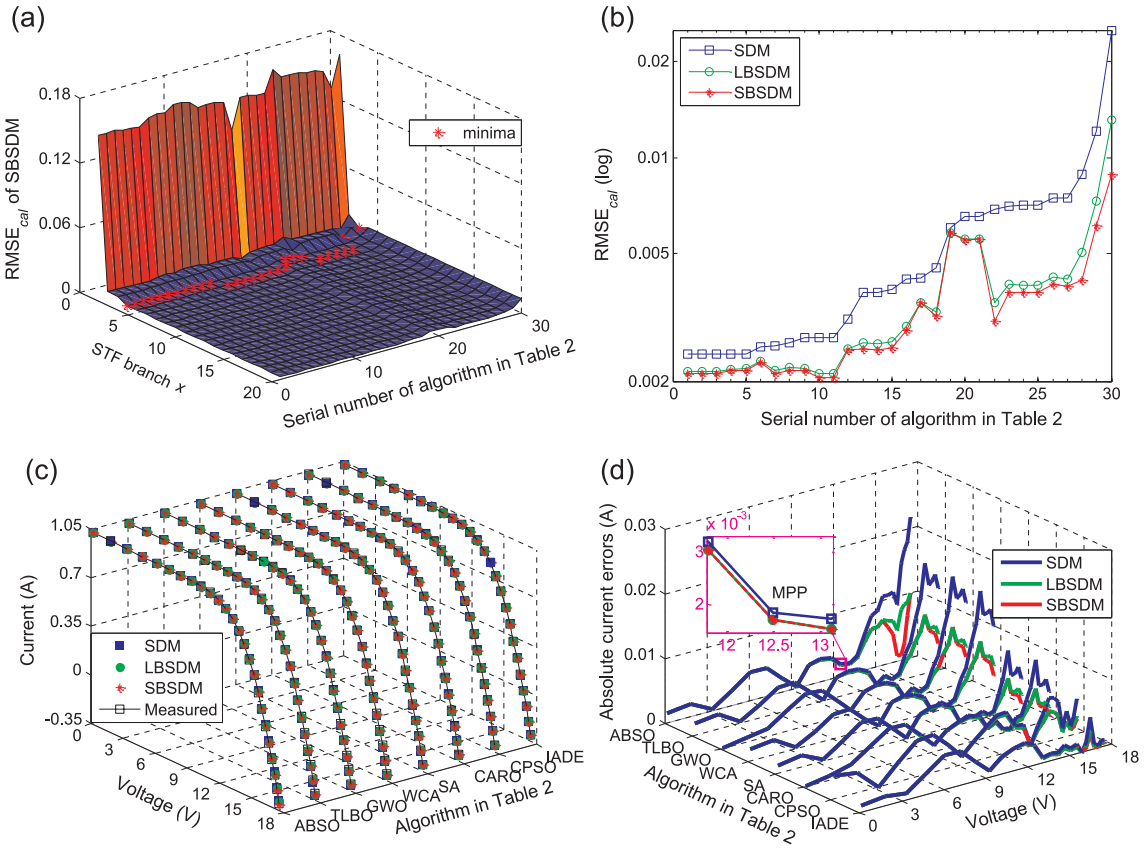

Fig. 3. Calculated curves of SDM, LBSDM and SBSDM using the measured *I–V* data of Photowatt-PWP 201 solar module [28] and the parameter values extracted by various algorithms in Table 2: (a) RMSE$_{cal}$ values of SBSDM at different STF branch *x*, (b) Comparison of RMSE$_{cal}$ values, (c) *I–V* characteristics and (d) absolute current errors.

load scanning experiment was set up to measure the *I–V* data of two solar modules: mono-crystalline STM6-40/36 and polycrystalline STP6-120/36. Both solar modules contain 36 cells in series, while operating at 51 °C and 55 °C respectively. These two sets of measured *I–V* data are very typical, because both of them lack the measurements near open-circuit voltage, as shown by Figs. 4(a) and 5(a). This means that the advantage of SBSDM and LBSDM will be heavily discounted in high voltage range. The parameter values reported in [51] and the RMSE$_{cal}$ values calculated from these two sets of measured *I–V* data are listed in Table 3.

Similar to previous cases, one can see from the last column of Table 3 that there is still no dominant correlation between parameter values and optimal STF branch *x*. Also, SBSDM still provides the smallest RMSE$_{cal}$ values, despite lacking the measurements near open-circuit voltage. This shows that SBSDM can better fit the measured *I–V* datasets and its accuracy is universal and reliable. Moreover, the zoomed-in views of Figs. 4 and 5 demonstrate that SBSDM acquires the smallest absolute current errors around MPP, followed by LBSDM and SDM. Although the difference between the absolute current errors of SBSDM and LBSDM is vanishingly small, but it can result in non-

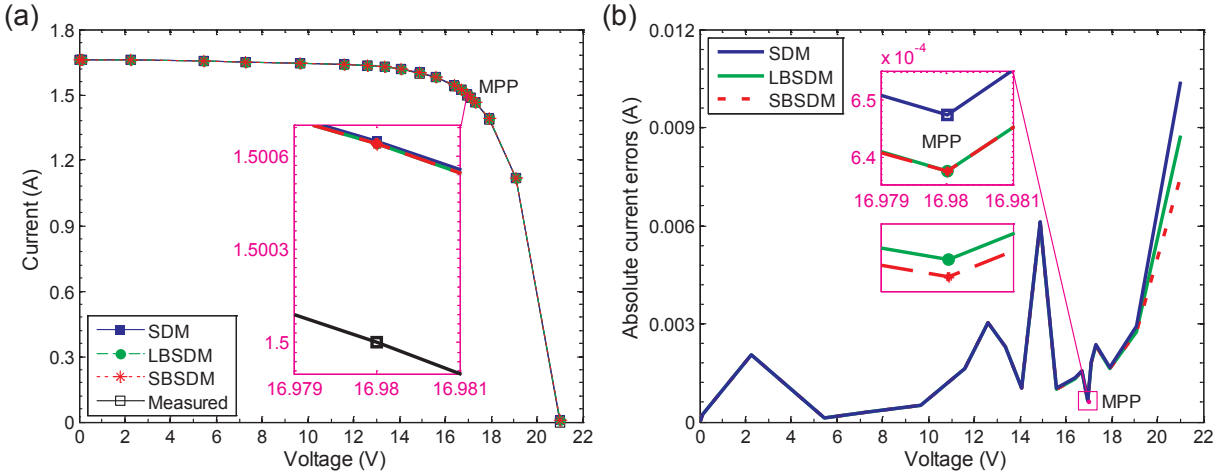

Fig. 4. Calculated curves of SDM, LBSDM and SBSDM using the measured *I–V* data of mono-crystalline STM6-40/36 module and parameter values reported in [51]: (a) *I–V* characteristics and (b) Absolute current errors.

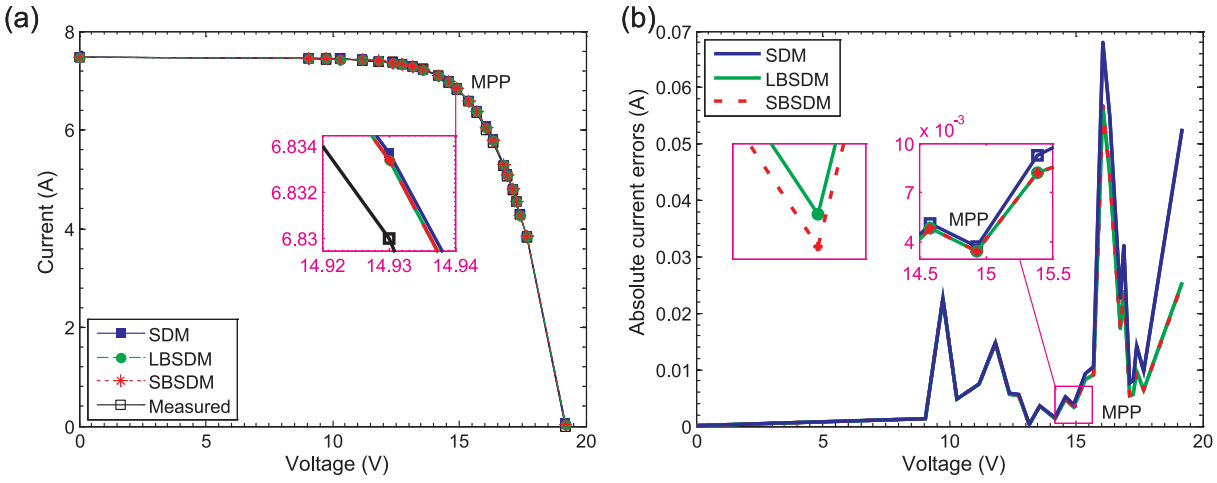

Fig. 5. Calculated curves of SDM, LBSDM and SBSDM using the measured *I–V* data of polycrystalline STP6-120/36 module and parameter values reported in [51]: (a) *I–V* characteristics and (b) absolute current errors.

Table 3
RMSE$_{cal}$ values of SDM, LBSDM and SBSDM calculated using the measured datasets of mono-crystalline STM6-40/36 module, polycrystalline STP6-120/36 module and the parameter values reported in [51].

Solar modules	Parameters					RMSE$_{cal}$			
	I_{ph} (A)	I_0 (μA)	n	R_s (mΩ)	R_{sh} (Ω)	SDM	LBSDM	SBSDM	Optimal x
STM6-40/36	1.6635	1.4142	1.4986	4.879	15.419	3.1185E−03	2.8370E−03	2.6510E−03	2
STP6-120/36	7.4838	1.2	1.2072	4.9	9.745	2.3710E−02	1.8250E−02	1.8237E−02	7

negligible absolute power errors in PV system.

All above results indicate that, the explicit multi-branch of STF endows SBSDM better fitness than LBSDM and SDM in representing the *I–V* characteristics of solar cell/modules. This superiority is independent on cell technologies, which is beneficial to providing a closer prediction of actual MPP and hence increase the efficiency of PV systems. Furthermore, this superiority will exert significant influence on the accuracy of parameter extraction of SBSDM.

3. Objective function for parameter extraction of three models

Before proceeding to evaluate the parameter extraction performance of SBSDM, LBSDM and SDM, an objective function should be first formulated. The main objective for parameter extraction of the three models is to find a set of parameter values and an appropriate STF branch x to minimize the errors between the calculated current and measured current. For easy comparison with previous literatures, RMSE$_{cal}$ is chosen as the objective function and the optimization goal is set to minimize Eq. (11) with respect to STF branch x and the unknown parameter vector $X = [I_{ph}, I_0, n, R_s, R_{sh}]$.

$$F(x, X) = RMSE_{cal}(x, X) = \underset{\substack{\mathbf{X}\in[LB,UB]\subset\mathbb{R}^+ \\ x\in\{1,\ 2,\ \ldots,\ 20\}\subset\mathbb{Z}^+}}{\text{minimize}} \sqrt{\frac{1}{N}\sum_{i=1}^{N} f_{\mathrm{M}}(V, I, x, X)^2} \tag{11}$$

where LB and UB are the lower and upper bounds on parameter vector X, respectively. N is the number of measured *I–V* data. x is the STF branch, which is exclusive for SBSDM. The error function $f_{\mathrm{M}}(V, I, x, X)$ can be formulated by Eqs. (12), (13) and (14) for SDM, LBSDM and SBSDM, respectively.

$$f_{\mathrm{SDM}}(V, I, X) = I_{ph} - I_0\left[\exp\left(\frac{V + IR_s}{nV_{th}}\right) - 1\right] - \frac{V + IR_s}{R_{sh}} - I \tag{12}$$

$$f_{\mathrm{LBSDM}}(V, I, X) = \frac{R_{sh}(I_{ph} + I_0) - V}{R_s + R_{sh}} - \frac{nV_{th}}{R_s}W_0(U) - I \tag{13}$$

$$f_{\mathrm{SBSDM}}(V, I, x, X) = \frac{R_{sh}(I_{ph} + I_0) - V}{R_s + R_{sh}} - \frac{nV_{th}}{R_s}trans_+(x, U) - I \tag{14}$$

It is evident from Eq. (11) that the smaller the RMSE$_{cal}$ value, the more accurate the parameter values extracted from the model. It should be noted that the parameter vector $X = [I_{ph}, I_0, n, R_s, R_{sh}]$ in Eqs. (12)–(14) is unknown to be extracted from the measured *I–V* data, whereas I_{ph}, I_0, n, R_s, R_{sh} are known in Eqs. (6)–(8).

4. Modified Nelder-Mead simplex (MNMS) algorithm

To investigate the parameter extraction performance of SBSDM and compare it to LBSDM and SDM, this section presents a modified Nelder-Mead simplex algorithm and a ranking based STF branch selection strategy for parameter extraction of them.

4.1. Outline of MNMS algorithm

As a pioneer of direct search, the Nelder-Mead simplex (NMS) algorithm delivers powerful efficiency for multidimensional unconstrained optimization without derivatives [64]. Basically, NMS algorithm minimizes the objective function of D-dimensional parameters by comparing one or two function evaluations at the $D + 1$ vertex of a nondegenerate simplex, and then updating the worst vertex by some combination of reflection, expansion, contraction and shrink, until encounters a (local, at least) minimum [65]. With respect to the premature termination of iterations, a heuristic approach is to restart several times with reasonably small number of iterations [64]. From these points of view, NMS is simple to understand, easy to program and very suitable for solving the parameter extraction problem of SBSDM, LBSDM and SDM.

In addition to the restart strategy mentioned above, five modifications are introduced in this section to improve the performance of

Table 4
Lower bound (LB) and upper bound (UB) on model parameters of the four solar cell/modules.

Model parameters	R.T.C France solar cell		Photowatt-PWP201 module		STM6-40/36 module		STP6-120/36 module	
Search ranges	LB	UB	LB	UB	LB	UB	LB	UB
I_{ph} (A)	0	1	0	2	0	2	0	8
I_0 (μA)	0	1	0	50	0	50	0	50
n	1	2	1	50	36	72	36	72
R_s (Ω)	0	0.5	0	2	0	2	0	2
R_{sh} (Ω)	0	100	0	2000	0	2000	0	2000

standard NMS algorithm, including selecting the start point from uniform sampling, sine bound handling method, weighted centroid, adaptive control parameters and greedy outside contraction. These modifications are interspersed in the main steps of proposed MNMS algorithm and outlined in Algorithm 1 for completeness.

Algorithm 1 (*Modified Nelder-Mead simplex*).

Input: MaxNFEs, initial STF branch x_0
1 Get the problem details: Model, ObjFun, LB, UB, D;
2 **if** Model ≡ SBSDM, **then** x= x_0, **else** x=NaN;
3 Set N_p=D×10, N_r=D×100, $Iter$=1, $Restart$=0;
4 % Step 1: Select start point X_0 from uniform sampling
5 P=LB+rand(N_p, D)·(UB−LB), F=ObjFun(x, P);
6 [F_0, id]=min(F), X_0=$P(id,:)$, $NFEs$=N_p;
7 **while** $NFEs \leq$ MaxNFEs **do**
8 % Step 2: Initialize simplex, see **Algorithm 2**
9 [$Su, S, F, NFEs$]=InitializeS($x, X_0, F_0, NFEs$);
10 $Iter$=$Iter$+1, $preset$=$Iter$+N_r;
11 % Step 3: Update simplex, see **Algorithm 3**
12 **while** $Iter < preset$ and $NFEs <$ MaxNFEs **do**
13 [S_u,S,F, $NFEs$]=UpdateS(x,S_u,S,F, $NFEs$);
14 $Iter$=$Iter$+1;
15 [F, id]=sort(F), S_u=$S_u(id,:)$, S=$S(id,:)$;
16 X_0=$S(1,:)$, F_0=$F(1)$, $Restart$=$Restart$+1;
17 % Step 4: Update STF branch x, see **Algorithm 4**
18 **if** Model ≡ SBSDM **then**
19 [x, F_0, $NFEs$]=Updatex(x_0, X_0, $NFEs$);
20 $Iter$=$Iter$+1;
Output: optimal STF branch x, X_{best}=X_0, F_{best}=F_0;

One can see from Algorithm 1 that the proposed MNMS algorithm begins with a uniform sampling of N_p points to select the start point X_0 (see step 1). Then in step 2, the start point X_0 is employed to initialize the unconstrained simplex S_u and its counterpart, the bound constrained simplex S. After the allowed N_r iterations of simplex transformation in step 3, for parameter extraction of SDM and LBSDM, the best vertex of the updated simplex is selected as the new start point X_0 and returned back to step 2 for restart. For parameter extraction of SBSDM, the new start point X_0 is also used to update the STF branch x before returning back to step 2 for restart. This restart process is repeated until the stop criterion, i.e. the maximum number of function evaluations (MaxNFEs) is met. The main steps of proposed MNMS algorithm are illustrated in Algorithms 2-4 and explained as below.

4.2. Main steps of MNMS algorithm

Step 1: Select start point X_0 from uniform sampling

For standard NMS algorithm, the first step should do is to give a starting guess, that is, a D-vector of model parameters as the start point to try. In order to decrease the sensibility to start point and reduce the probability of being trapped in local minima, the uniform sampling with default random seeds is used to generate $N_p = D \times 10$ points spanning the entire search space of [LB, UB]. Then the point, which has the lowest function value F_0 is selected as the initial start point X_0. This modification essentially is a controlled random search procedure, which can avoid the empirical selection of start point and thus ensure the reproducibility of proposed MNMS algorithm. This step is programmed in lines 5 and 6 of Algorithm 1, where P denotes the population of N_p sample points, D is the dimensionality of parameter vector X, rand(N_p, D) is an N_p-by-D matrix containing D uniformly distributed random real number in (0, 1), and *NFEs* denotes the number of function evaluations.

Step 2: Initialize simplex

Since NMS algorithm does not allow bound constraints, this step begins with converting the bound constrained X_0 into its unconstrained surrogate X_{u0} via Eqs. (15) and (16), as is programmed in lines 4 and 5 of Algorithm 2. The 2π in the right side of Eq. (16) is used to prevent the premature termination of iterations caused by simplex degeneration, which is in well accordance with the viewpoint of [66]. Then in line 7 of Algorithm 2, X_{u0} and X_0 are assigned to be the first vertex of unconstrained simplex S_u and bound constrained simplex S, respectively. For unconstrained simplex S_u, the remaining D vertex are generated around X_{u0} according to Eq. (17), where j = 1, 2, …, D, e_j is the unit vector in the j^{th} coordinate direction, Δ_j is a small constant chosen from Eq. (18). For bound constrained simplex S, the last D vertex are constrained within the search space [LB, UB] via Eqs. (19) and (20) and just in case of overflow or underflow. This initialization process is programmed in lines 8 to17 of Algorithm 2, where the SineBound function denotes the bounding operations via Eqs. (19) and (20). Since the arcsine function in Eq. (16) and sine function in Eq. (19) are used to convert the bound constrained problem into its unconstrained form, we name this trick as the sine bound handling method, which is mainly derived from the idea of [67].

$$X_{u0} = 2(X_0 - \mathrm{LB})/(\mathrm{UB} - \mathrm{LB}) - 1 \tag{15}$$

$$X_{u0} = 2\pi + \mathrm{asin}(\max(-1, min(1, X_{u0}))) \tag{16}$$

$$S_{uj+1} = X_{u0} + \Delta_j e_j \tag{17}$$

$$\Delta_j = \begin{cases} 0.05 & \text{if} X_{u0}(j) \neq 0 \\ 0.00025 & \text{if} X_{u0}(j) = 0 \end{cases} \tag{18}$$

$$S_{j+1} = LB + 0.5(UB - LB)[\sin(S_{uj+1}) + 1] \tag{19}$$

$$S_{j+1} = max(LB, min(UB, S_{j+1})) \tag{20}$$

Algorithm 2 (*Initialize simplex*).

```
1  function [S_u,S,F,NFEs]=InitializeS(x,X_0,F_0,NFEs)
2      Get the problem details: ObjFun, LB, UB, D;
3      % Convert X_0 into unconstrained surrogate X_u0
4      X_u0=2((X_0−LB)./(UB−LB))−1;
5      X_u0=2π+asin(max(−1, min(1, X_u0)));
6      % Initialize simplex using X_u0, X_0 and F_0
7      S_u(1, :)=X_u0,  S(1, :)=X_0,  F(1)=F_0;
8      for j = 1 to D do
9          y=X_u0;
10         if y(j) ≠ 0 then
11             y(j)=(1+0.05)y(j);
12         else
13             y(j)=0.00025;
14         S_u(j+1, :)=y;
15         S(j+1, :)=SineBound(y, LB, UB);
16         F(j+1)=ObjFun(x, S(j+1, :))
17         NFEs=NFEs+1;
18     return
```

Step 3: Update simplex

One iteration of the proposed MNMS algorithm consists of the following sub-steps, where the operation of converting the unconstrained point into its bound-constrained surrogate, i.e. Eqs. (19) and (20) must be held accountable for the simplex transformations.

(a) Ordering: sort the D + 1 vertex in order of increasing function values satisfying $F(1) \leq F(2) \leq \ldots \leq F(\mathrm{D}) \leq F(\mathrm{D}+1)$, as is programmed in line 3 of Algorithm 3.

(b) Weighted centroid: In proposed MNMS algorithm, the weighted centroid formulated by Eq. (21) is adopted to replace the traditional centroid $c = \sum_{k=1}^{\mathrm{D}} S_{uk}/\mathrm{D}$ in standard NMS, as is programmed in line 4 of Algorithm 3. The effectiveness of this modification has been proved by the analog design optimization in [68].

$$wc = \sum_{k=1}^{\mathrm{D}} \left\{ S_{uk} \Big/ \left[F_k \sum_{k=1}^{\mathrm{D}} (1/F_k) \right] \right\} \tag{21}$$

(c) Adaptive control parameters: In proposed MNMS algorithm, the empirical control parameters in standard NMS algorithm, i.e. $\alpha = 1$ for reflection, $\beta = 2$ for expansion, $\gamma = 0.5$ for contraction and $\delta = 0.5$ for shrinkage are replaced with the adaptive control parameters formulated by Eq. (22), as is programmed in line 5 of Algorithm 3. According to [66], the adaptive β contributes to preventing the simplex from bad distortion, the adaptive γ helps to alleviate the reduction of simplex diameter and the adaptive δ is to prevent the simplex diameter from sharp reduction, the effectiveness of which have been proved by [5].

$$\alpha = 1, \quad \beta = 1 + \frac{2}{D}, \quad \gamma = 0.75 - \frac{1}{2D}, \quad \delta = 1 - \frac{1}{D} \tag{22}$$

(d) Reflection: Compute the unconstrained reflection point S_{ur} using Eq. (23) and convert it into the bound-constrained reflection point S_r via Eqs. (19) and (20). If $F(1) \leq F_r < F(\mathrm{D})$, replace $S_{u\mathrm{D}+1}$ with

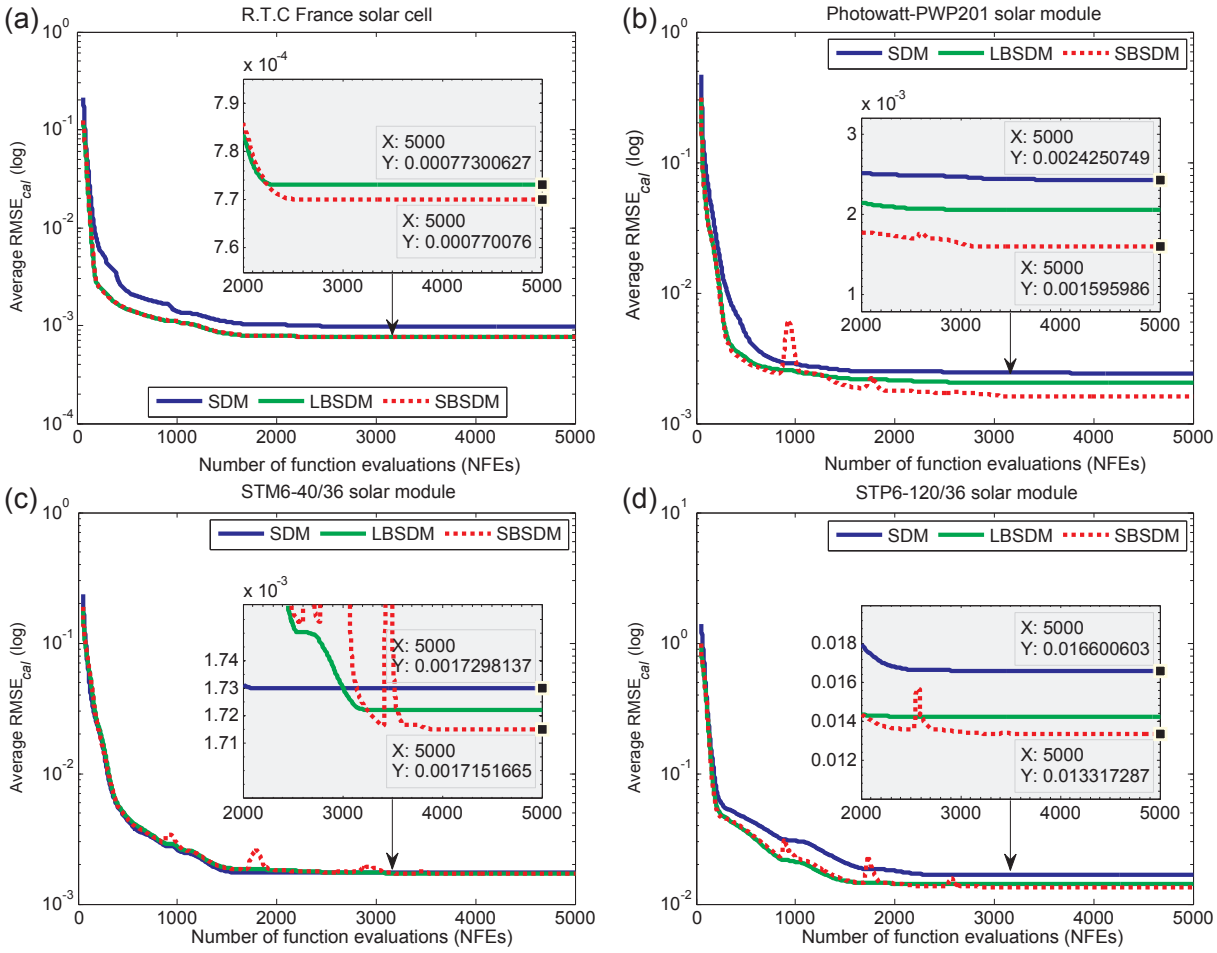

Fig. 6. The average convergence curves of 100 independent runs of MNMS algorithm during the parameter extraction process of SDM, LBSDM and SBSDM of four solar cell/modules.

S_{ur}, S_{D+1} with S_r and go to next iteration, as is programmed in lines 6, 7, 13 and 14 of Algorithm 3. Otherwise, perform an expansion transformation.

$$S_{ur} = (1 + \alpha)wc - \alpha S_{uD+1} \tag{23}$$

(e) Expansion: If $F_r < F(1)$, compute the unconstrained expansion point S_{ue} using Eq. (24) and convert it into the bound-constrained expansion point S_e via Eqs. (19) and (20). If $F_e < F_r$, replace S_{uD+1} with S_{ue}, S_{D+1} with S_e and go to next iteration. Otherwise, replace S_{uD+1} with S_{ur}, S_{D+1} with S_r and go to next iteration, as is programmed in lines 8–12 of Algorithm 3.

$$S_{ue} = (1 + \beta)wc - \beta S_{uD+!} \tag{24}$$

(f) Outside contraction: If $F(D) \le F_r < F(D + 1)$, compute the unconstrained contraction point S_{uoc} using Eq. (25) and convert it into the bound-constrained contraction point S_{oc} via Eqs. (19) and (20). If $F_{oc} \le F_r$, replace S_{uD+1} with S_{uoc}, S_{D+1} with S_{oc} and go to next iteration. Otherwise, replace S_{uD+1} with S_{ur}, S_{D+1} with S_r and go to next iteration, as is programmed in lines 15–19 of Algorithm 3. Special needs to be pointed out that the rear half of this sub-step is different from that of the standard NMS, where NMS performs a shrinkage transformation if outside contraction failed. The reason for excluding original shrinkage transformation is that, the function value at reflection point satisfies $F_r < F(D + 1)$ and there is no further function evaluation needed [4]. Therefore, this modification is essentially a greedy outside contraction.

$$S_{uoc} = (1 + \gamma)wc - \gamma S_{uD+1} \tag{25}$$

Algorithm 3 (*Update simplex*).

```
1  function [S_u, S, F, NFEs]=UpdateS(x, S_u, S, F, NFEs)
2      Get the problem details: ObjFun, LB, UB, D;
3      [F, id]=sort(F),  S_u=S_u(id, :),  S=S(id, :);        % Ordering
4      wc=sum(S_u(1:D, :)./ repmat((F(1:D)·sum(1./F(1:D)))', [1, D]);  % Weighted centroid
5      α=1,  β=1+2/D,  γ=0.75−1/(2D),  δ=1−1/D;   % Adaptive control parameters
6      S_ur=(1+α)wc−αS_u(D+1)),  S_r=SineBound(S_ur, LB, UB);        % Reflection
7      F_r=ObjFun(x, S_r),  NFEs=NFEs+1;
8      if F_r < F(1) then   % Expansion
9          S_ue=(1+ αβ)wc−αβS_u(D+1)),  S_e= SineBound(S_ue, LB, UB);
10         F_e=ObjFun(x, S_e),  NFEs=NFEs+1;
11         if F_e < F_r then  S_u(D+1)=S_ue ,  S(D+1)=S_e ,  F(D+1)=F_e;
12         else  S_u(D+1, :)=S_ur ,  S(D+1, :)=S_r ,  F(D+1)=F_r;
13     else if F_r < F(D) then
14         S_u(D+1, :)=S_ur ,  S(D+1, :)=S_r ,  F(D+1)=F_r;
15         else if F_r < F(D+1) then   % Outside contraction
16             S_uoc=(1+ αγ)wc−αγS_u(D+1)),  S_oc=SineBound(S_uoc, LB, UB);
17             F_oc=ObjFun(x, S_oc),  NFEs=NFEs+1;
18             if F_oc ≤ F_r then  S_u(D+1, :)=S_uoc ,  S(D+1, :)=S_oc ,  F(D+1)=F_oc;
19             else  S_u(D+1, :)=S_ur,  S(D+1, :)=S_r,  F(D+1)=F_r;
20         else  % Inside contraction
21             S_uic= (1−γ)wc+γS_u(D+1)),  S_ic= SineBound(S_uic, LB, UB);
22             F_ic=ObjFun(x, S_ic),  NFEs=NFEs+1;
23             if F_ic < F(D+1) then  S_u(D+1, :)=S_uic,  S(D+1, :)=S_ic,  F(D+1)=F_ic;
24             else  % Shrinkage
25                 for i = 2 to D+1 do
26                     S_u(i, :)=S_u(1, :) + δ(S_u(i, :)−S_u(1, :));
27                     S(i, :)=SineBound (S_u(i, :),  LB,  UB);
28                     F(i)=ObjFun(x, S(i, :)),  NFEs=NFEs+1;
29     return
```

(g) Inside contraction: If $F_r \ge F(D + 1)$, compute the unconstrained contraction point S_{uic} using Eq. (26) and convert it into the bound-constrained contraction point S_{ic} via Eqs. (19) and (20). If $F_{ic} < F(D + 1)$, replace S_{uD+1} with S_{uic}, S_{D+1} with S_{ic} and go to next iteration. Otherwise, perform a shrinkage transformation, as is programmed in lines 20–24 of Algorithm 3.

$$S_{uic} = (1-\gamma)wc + \gamma S_{uD+1} \tag{26}$$

(h) Shrinkage: For $2 \le i \le D + 1$, create D new unconstrained vertex S_{ui} using Eq. (27) and convert them into their bound-constrained surrogates S_i via Eqs. (19) and (20). Then update the current simplex with the D new vertex, as is programmed in lines 25–28 of Algorithm 3.

$$S_{ui} = S_{u1} + \delta(S_{ui} - S_{u1}) \tag{27}$$

The next iteration begins with the new unconstrained simplex until the allowed number of iterations is reached.

Step 4: Ranking based STF branch selection strategy

Table 5
Statistical results of 100 independent runs of MNMS algorithm for parameter extraction of SDM, LBSDM and SBSDM of four solar cell/modules.

Models	NFE_{th}		CPU time (s)		Minimum $RMSE_{cal}$			
	Mean	Std	Mean	Std	Min	Mean	Max	Std
R.T.C France solar cell [28]	thV = 0.001							
SDM	1472	501	0.061	0.002	9.860219E−04	9.860219E−04	9.860219E−04	3.916409E−17
LBSDM	946	439	0.220	0.003	7.730063E−04	7.730063E−04	7.730063E−04	1.747686E−17
SBSDM	981	434	0.138	0.013	7.699621E−04	7.700760E−04	7.728095E−04	5.607788E−07
Photowatt-PWP201 module [28]	thV = 0.01							
SDM	282	225	0.066	0.004	2.425075E−03	2.425075E−03	2.425075E−03	2.169031E−17
LBSDM	227	128	0.223	0.003	2.052961E−03	2.052961E−03	2.052961E−03	2.332851E−17
SBSDM	215	82	0.127	0.005	1.595986E−03	1.595986E−03	1.595986E−03	1.634395E−17
STM6-40/36 module [51]	thV = 0.002							
SDM	1186	289	0.064	0.002	1.729814E−03	1.729814E−03	1.729814E−03	8.457956E−18
LBSDM	1180	386	0.216	0.002	1.721922E−03	1.721922E−03	1.721922E−03	8.552746E−18
SBSDM	1192	382	0.096	0.005	1.715166E−03	1.715166E−03	1.715166E−03	7.709157E−18
STP6-120/36 module [51]	thV = 0.02							
SDM	1349	484	0.070	0.003	1.660060E−02	1.660060E−02	1.660060E−02	1.249804E−16
LBSDM	905	343	0.227	0.003	1.425106E−02	1.425106E−02	1.425106E−02	1.070273E−16
SBSDM	943	388	0.128	0.005	1.331729E−02	1.331729E−02	1.331729E−02	1.047479E−16

For parameter extraction of SBSDM, there is an additional problem of searching appropriate STF branch x to minimize the objective function. In order to facilitate the selection of start point X_0, one can see from Algorithm 1 that an initial STF branch x_0 needs to be given at the beginning of proposed MNMS algorithm. During the first loop of Step 2 and Step 3, STF branch x is fixed at initial x_0 to minimize the objective function of SBSDM. Considering the fact that the optimal STF branch x in Tables 1–3 is generally less than or equal to 7, the median $x_0 = 4$ is empirically specified for parameter extraction of R.T.C. France solar cell and mono-crystalline STM6-40/36 module, while assigning $x_0 = 7$ for parameter extraction of Photowatt- PWP201 and STP6-120/36 modules. Within the subsequent restart loops, one can see from Algorithm 4 that a ranking based selection strategy is adopted to periodic update STF branch x for parameter extraction of SBSDM. The main idea is that

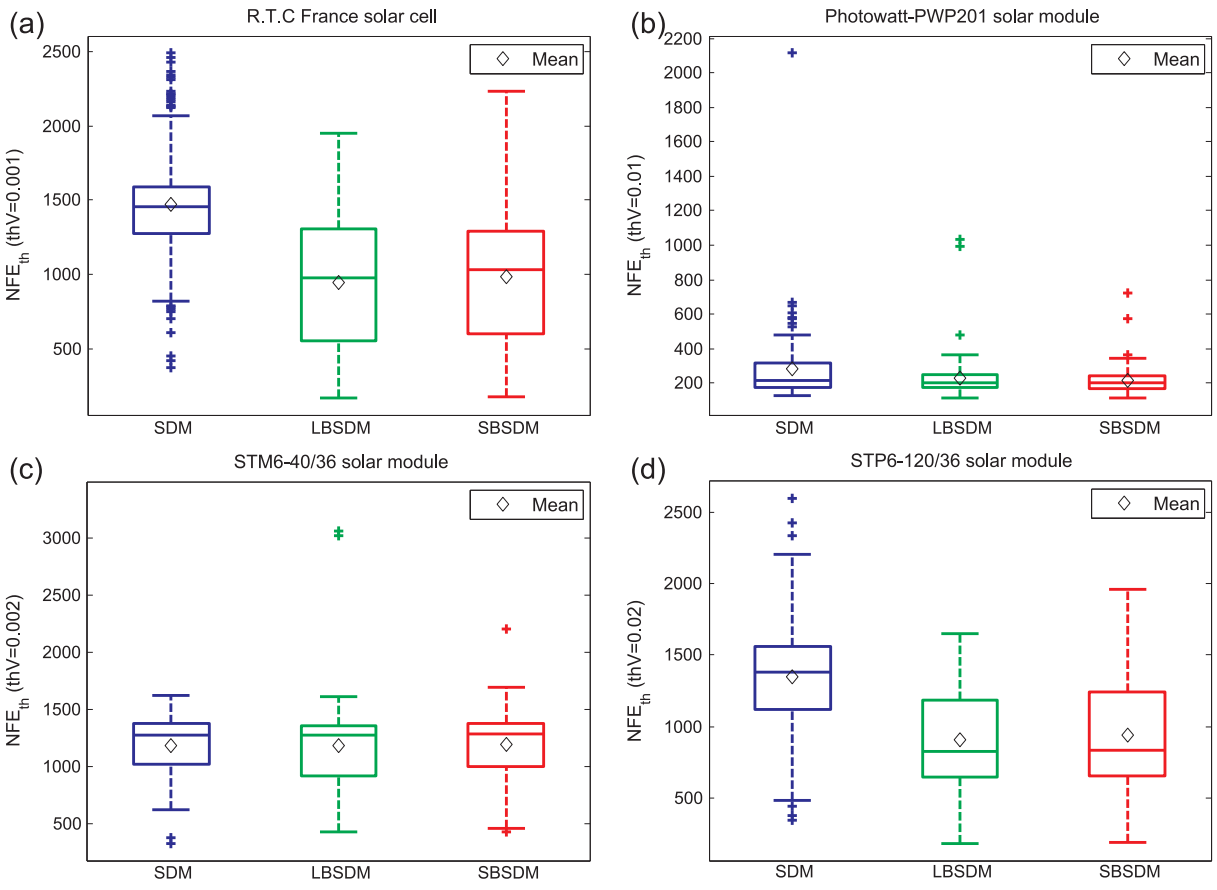

Fig. 7. Box plots of the number of function evaluations at which the $RMSE_{cal}$ is equal or less than the threshold value (thV) over the 100 independent runs of MNMS algorithm for parameter extraction of SDM, LBSDM and SBSDM of four solar cell/modules.

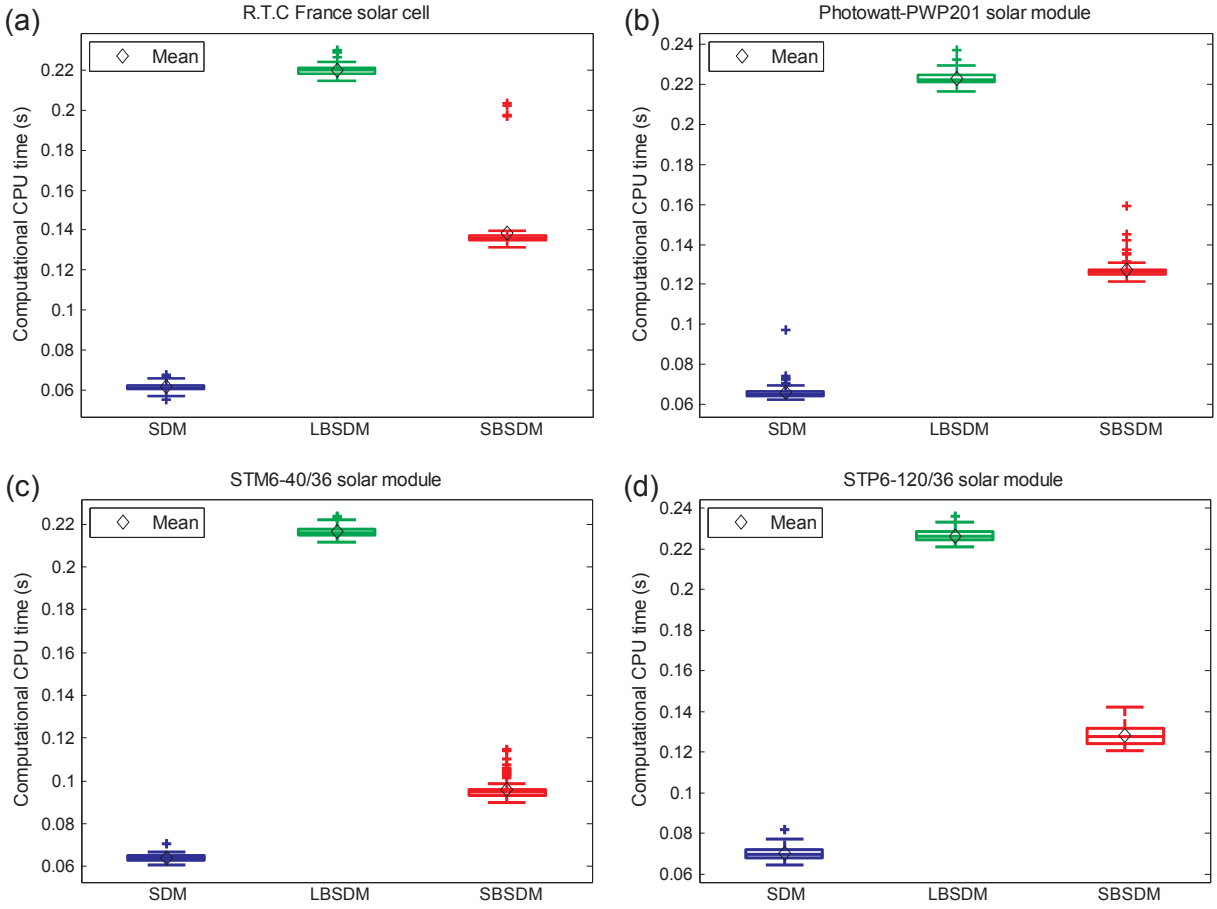

Fig. 8. Box plots of the computational CPU time over 100 independent runs of MNMS algorithm for parameter extraction of SDM, LBSDM and SBSDM of four solar cell/modules.

within the integer interval $x \in [1, x_0]$, if there is no valley point of the function values, the positive integer k corresponding to the lowest function value at fixed X_0 is selected as the optimal STF branch x for parameter extraction of next loop. Otherwise, the rounded mean value of all valley points minus one is assigned as the optimal STF branch x. It should be pointed out that although above strategy is derived from trial-and-error experiments, the fundamental insight behind it is the divide-and- conquer strategy commonly used in branch and bound method.

Algorithm 4 (*Update STF branch x*).

```
function [x, F0, NFEs]=Updatex(x0, X0, NFEs)
    for k = 1 to 20 do
        F(k)=ObjFun(k, X0)
        NFEs=NFEs+1
    valleypoint=find(diff(F(1:x0))>0);
    if isempty(valleypoint) then
        [F0, x]=min(F);
    else
        x=round(mean(valleypoint))−1;
        F0=F(x);
    return
```

Step 5: Implement restart strategy with allowed number of iterations

As mentioned in [64], NMS can take an enormous amount of reflections with negligible improvement in function value, despite being nowhere near to a minimum. This usually results in premature termination of iterations. In this scenario, it is frequently a good idea to restart the algorithm several times. In this paper, the allowed number of iterations is set to be $N_r = D \times 100$ to decide whether to restart or not, as is programmed in lines 10 and 12 of Algorithm 1. For each restart, the optimal parameter values returned from previous loop are accepted as the new start point X_0 to further minimize the objective function and thus improve the solution quality. After several restarts, MNMS algorithm is terminated once MaxNFEs is reached/exceeded.

5. Parameter extraction comparison of three models

This section compares the parameter extraction performance of SBSDM, LBSDM and SDM in default Matlab environment using proposed MNMS algorithm. To ensure fair comparison, MNMS algorithm is implemented under the same simulation conditions, i.e. the search ranges and stop criterion are kept the same in parameter extraction of SBSDM, LBSDM and SDM. The search ranges for standard datasets of R.T.C France solar cell and Photowatt-PWP201 module [28] are set the same as [25–63] and given in Table 4. According to the well extracted parameter values reported in [51] and similar to the boundary of standard datasets, the search ranges for practical measured datasets of STM6- 40/36 and STP6-120/36 modules [51] are set as Table 4. The stop criteria of MNMS algorithm is set to be MaxNFEs = 5000. In order to speed up the computation of Lambert W function, the

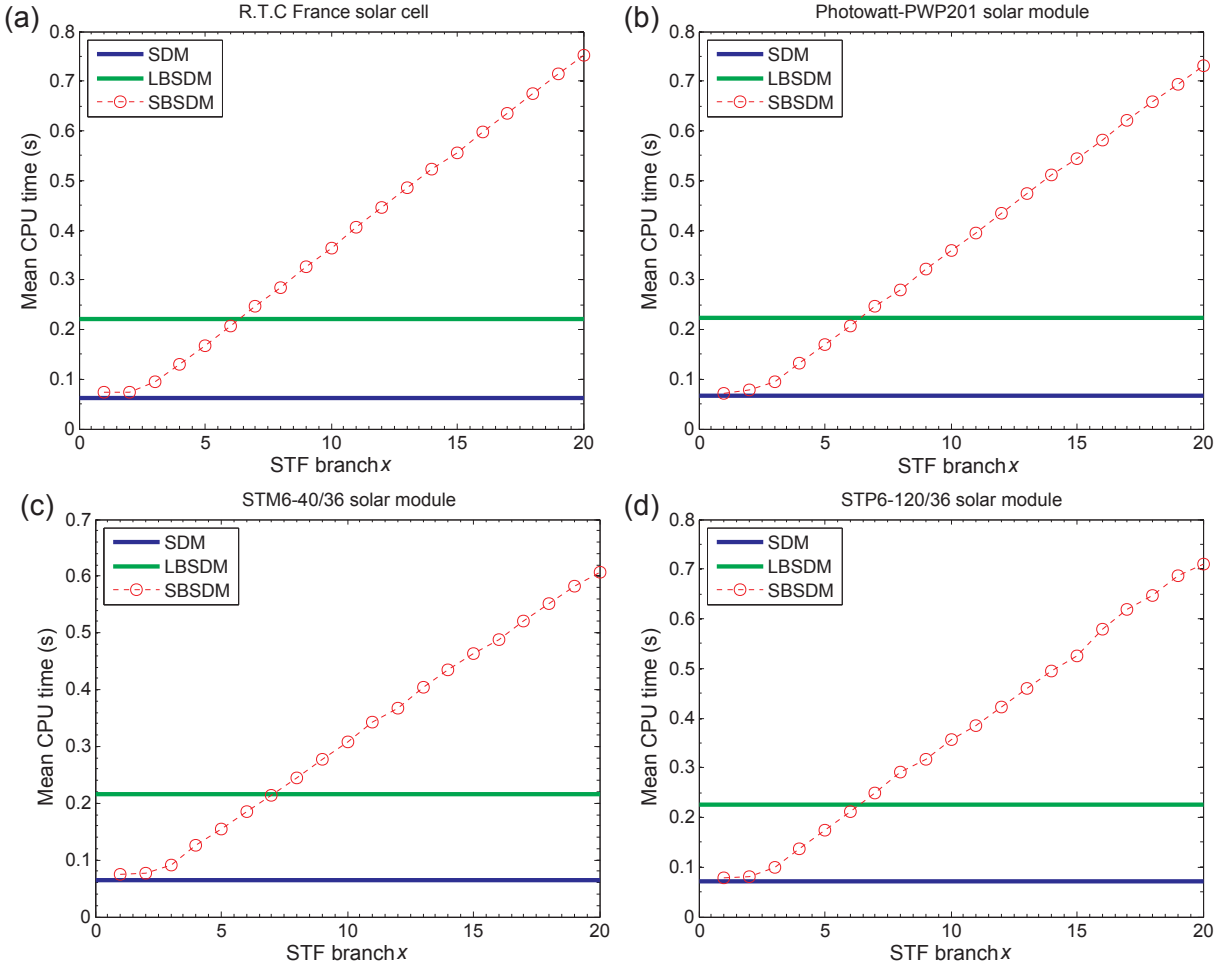

Fig. 9. Mean CPU time derived from fixed x in parameter extraction of SBSDM of four solar cell/modules. For easy comparison and crosschecking, the mean CPU time of SDM and LBSDM are also plotted here.

pvl_lambertw.m file [69] developed by the PV Performance Modeling Collaborative group at Sandia National Laboratories is adopted in parameter extraction of LBSDM. For reducing the computational efforts of $trans_+(x, U)$ in Eq. (5), the factorial of m wherein is coded by a lookup table method to improve the parameter extraction process of SBSDM. Furthermore, in order to achieve a higher confidence level of comparison results, 100 independent runs of MNMS algorithm are implemented for parameter extraction of above-mentioned four solar cell/modules. Convergence speed, computation time, robustness and accuracy are chosen as the performance criteria to evaluate the parameter extraction results of SBSDM, LBSDM and SDM. All comparative experiments were carried on a personal laptop with an Intel Core i5-4300 M processor @ 2.60 GHz, 4 GB RAM, under the Windows 7 64-bit OS.

5.1. Convergence speed

The average convergence curves of 100 independent runs of MNMS algorithm are illustrated in Fig. 6, indicating different average $RMSE_{cal}$ values during the parameter extraction process of SBSDM, LBSDM and SDM of the four solar cell/modules. It is evident from Fig. 6 that in almost the whole process, the average $RMSE_{cal}$ value of SDM is bigger than that of LBSDM and SBSDM. This can be attributed to the inherently implicit nature of SDM, which increases the difficulty of parameter extraction. In the early stage, there is almost no difference between LBSDM and SBSDM. However, it is clear from the zoomed-in view of Fig. 6 that LBSDM stagnates quickly, while SBSDM continues to converge toward the smallest average $RMSE_{cal}$ value. Just like ocean crests, the damped oscillations appeared in SBSDM curves reflect well on the tuning process of ranking based STF branch selection strategy presented in Algorithm 4. Each crest corresponds to a switchover process between different STF branches. Because of the sensibility of parameter values to STF branch, the crest values are not the same and decrease gradually to zero. According to the final average $RMSE_{cal}$ value, the convergence performance of the three models can be sorted as SBSDM ≥ LBSDM ≥ SDM. In other words, SBSDM needs fewer computational efforts to reach the same accuracy in comparison with LBSDM and SDM.

The statistical results of 100 independent runs of MNMS algorithm are summarized in Table 5, where NFE_{th} records the number of function evaluations at which the $RMSE_{cal}$ is equal or less than the threshold value (thV). From Table 5 and Fig. 7, it is obvious that SDM gets the

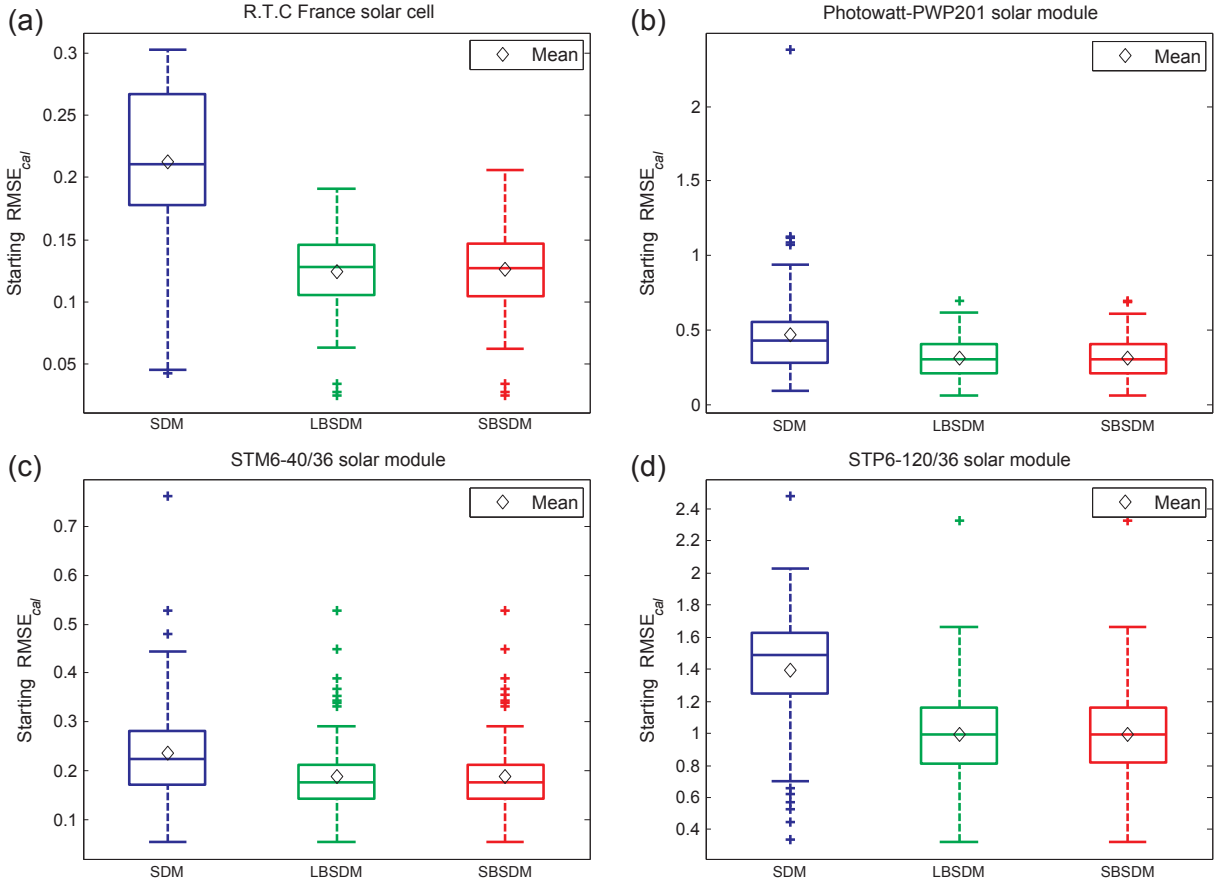

Fig. 10. Box plots of the starting RMSE$_{cal}$ values over 100 independent runs of MNMS algorithm for parameter extraction of SDM, LBSDM and SBSDM of four solar cell/modules.

worst convergence speed, because most of the mean NFE_{th} of SDM are bigger than those of LBSDM and SBSDM, while there is very little difference between LBSDM and SBSDM.

5.2. Computation time

Considering the fact that there is no great difference between the mean NFE_{th} of LBSDM and SBSDM, the computational CPU time is selected as another index for further examination of convergence speed. It is clear from Table 5 and Fig. 8 that the mean CPU time required for parameter extraction of LBSDM is more than 1.6 and 3.2 times slower than that of SBSDM and SDM, respectively. This suggests that the time computational efficiency of SBSDM is inferior to SDM but superior to LBSDM, which means SBSDM will allow a faster response time than LSBSDM for real-time optimal control of PV systems.

The mean CPU time derived from fixed SFT branch in parameter extraction of SBSDM of four solar cell/modules is depicted in Fig. 9. It is obvious that the larger the STF branch x, the more time required in parameter extraction of SBSDM, while the mean CPU time of LBSDM falls between the STF branches $x = 6$ and $x = 7$ of SBSDM. Due to the optimal STF branches (See next subsection) for the four solar cell/modules are less than $x = 6$, the parameter extraction process of SBSDM is time saving than that of LBSDM.

5.3. Robustness

Fig. 10 depicts the starting RMSE$_{cal}$ values over 100 independent runs of MNMS algorithm for parameter extraction of SDM, LBSDM and SBSDM of the four solar cell/modules. One can clearly see from Fig. 10 that SDM always provides the biggest mean starting RMSE$_{cal}$ value, while there is very little difference between LBSDM and SBSDM. This can be attributed to the fitness difference as already discussed in Section 2.

In terms of minimum RMSE$_{cal}$ values, it is obvious from Fig. 11 that all three models are very stable, except the SBSDM of R.T.C France solar cell indicating distinct vibrations. In Fig. 11(a), the minimum RMSE$_{cal}$ values for SBSDM of R.T.C France solar cell fall into two groups: 0.00076996211 via the optimal STF branch $x = 4$ and 0.00077280948 via the suboptimal STF branch $x = 6$, repeating 96 and 4 times respectively. This leads the standard deviation of minimum RMSE$_{cal}$ of SBSDM to be the biggest one in Table 5 and proves SBSDM is slightly less robust than LBSDM and SDM.

Furthermore, Fig. 11(a) also suggests that the ranking-based STF branch selection strategy in Algorithm 4 is not good enough to ensure the uniqueness of optimal x in parameter extraction of SBSDM. In order to investigate its validity, the minimum RMSE$_{cal}$ values derived from the fixed x for parameter extraction of SBSDM are depicted in Fig. 12. It is clear that the optimal STF branches are $x = 4$, $x = 3$, $x = 1$ and $x = 3$

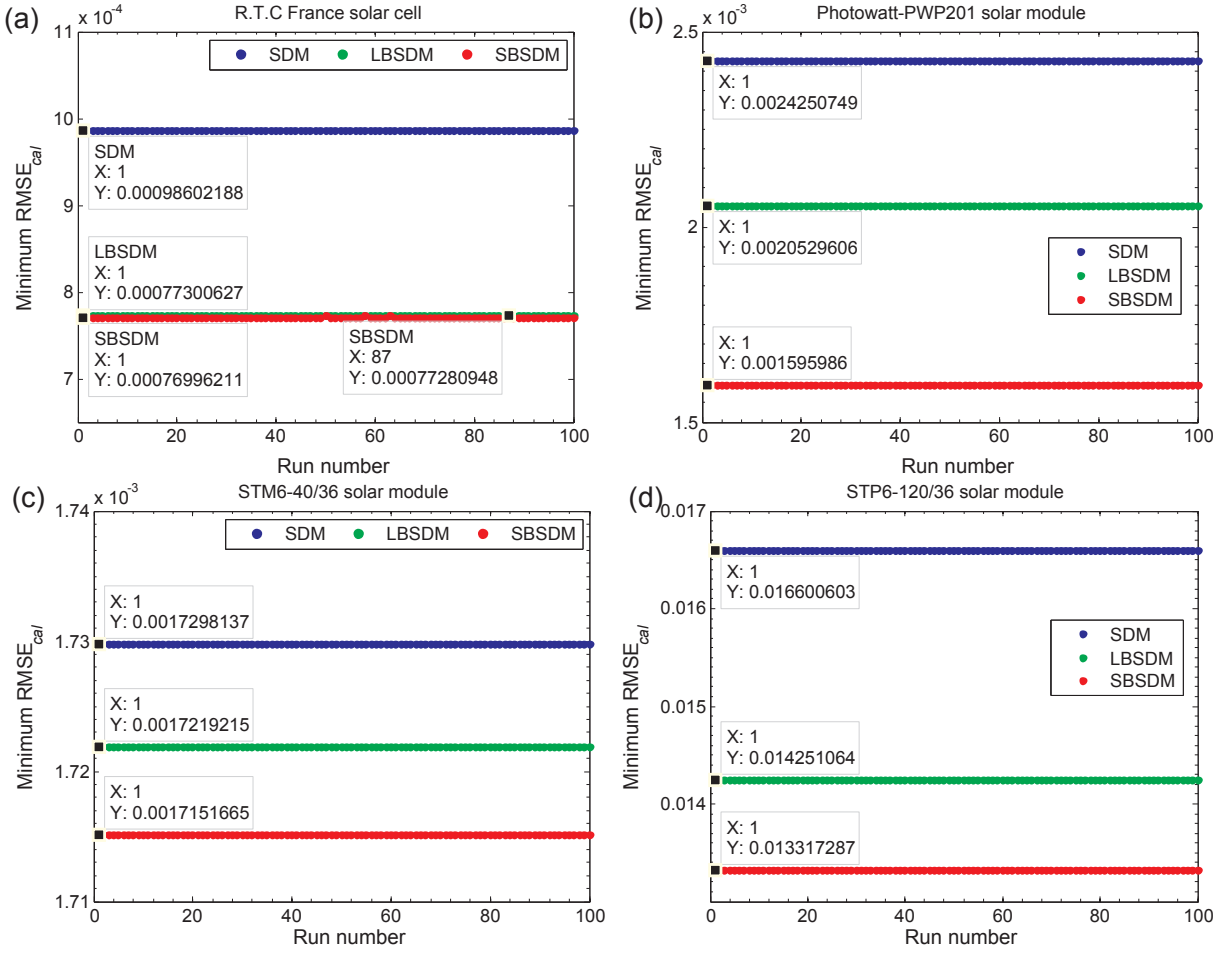

Fig. 11. Distribution of the minimum $RMSE_{cal}$ values over 100 independent runs of MNMS algorithm for parameter extraction of SDM, LBSDM and SBSDM of four solar cell/modules.

for the four solar cell/modules, respectively. A close inspection of the zoomed-in view of Fig. 11(a) reveals that in the case of R.T.C France solar cell, the suboptimal branch is $x = 6$, followed by $x = 7$. By crosschecking the minimum $RMSE_{cal}$ values in Figs. 11 and 12, it can be inferred that the ranking-based STF branch selection strategy is effective, because it can at least find the suboptimal STF branch $x = 6$, at which the minimum $RMSE_{cal}$ value of SBSDM is smaller than that of LBSDM.

5.4. Accuracy

The optimal parameter values and $RMSE_{cal}$ values extracted by MNMS algorithm for SDM, LBSDM and SBSDM of the four solar cell/modules are summarized in Table 6. It is clear that the optimal $RMSE_{cal}$ values of three models can be sorted as SBSDM < LBSDM < SDM, indicating that SBSDM consistently gets the most accurate parameter values among three models in all cases. In order to compare the quality of the optimal parameter values, they are back-substituted into Eqs. (1), (2) and (4) respectively to reconstruct the simulated current I_{sim} at the measured voltage point. As mentioned in [15], this is simply done by using *fzero* function or bisection method [5] or Newton method [30,38] when V is known while I is unknown. Note that the simulated current I_{sim} is different from the calculated current I_{cal} in Eqs. (6)–(8) where both V and I are known. The simulated I–V data of SDM, LBSDM and LBSDM, and their respective absolute current errors are shown in Fig. 13 and Tables 7–10 respectively.

It is evident from Fig. 13 that the simulated I–V data of SDM, LBSDM and SBSDM are all in good agreement with the measured I–V data. Nevertheless, the last lines of Tables 7–10 give evidence that SBSDM provides the smallest $RMSE_{sim}$ value, followed by LBSDM and SDM. This proves that the simulated I–V data of SBSDM is in best agreement with the measured I–V data, and further confirms that the optimal parameter values extracted from SBSDM are more accurate than those from LBSDM and SDM. It must be highlighted that due to the inherently implicit nature of SDM, whose $RMSE_{cal}$ values in Table 6 is always larger than its $RMSE_{sim}$ values in Tables 7–10. In contrast, due to the exact explicit nature of LBSDM and SBSDM, whose $RMSE_{cal}$ values are always identical with their respective $RMSE_{sim}$ values. Therefore, the above-mentioned reconstruction process of simulated current data is not at all necessary for LBSDM and SBSDM, since their simulated current data can be calculated in a direct and straightforward manner. With regard to the small difference among the $RMSE_{sim}$ values of SDM, LBSDM and LBSDM, it must be emphasized that any reduction of $RMSE_{sim}$ value is of vital significance, because it results in improvement

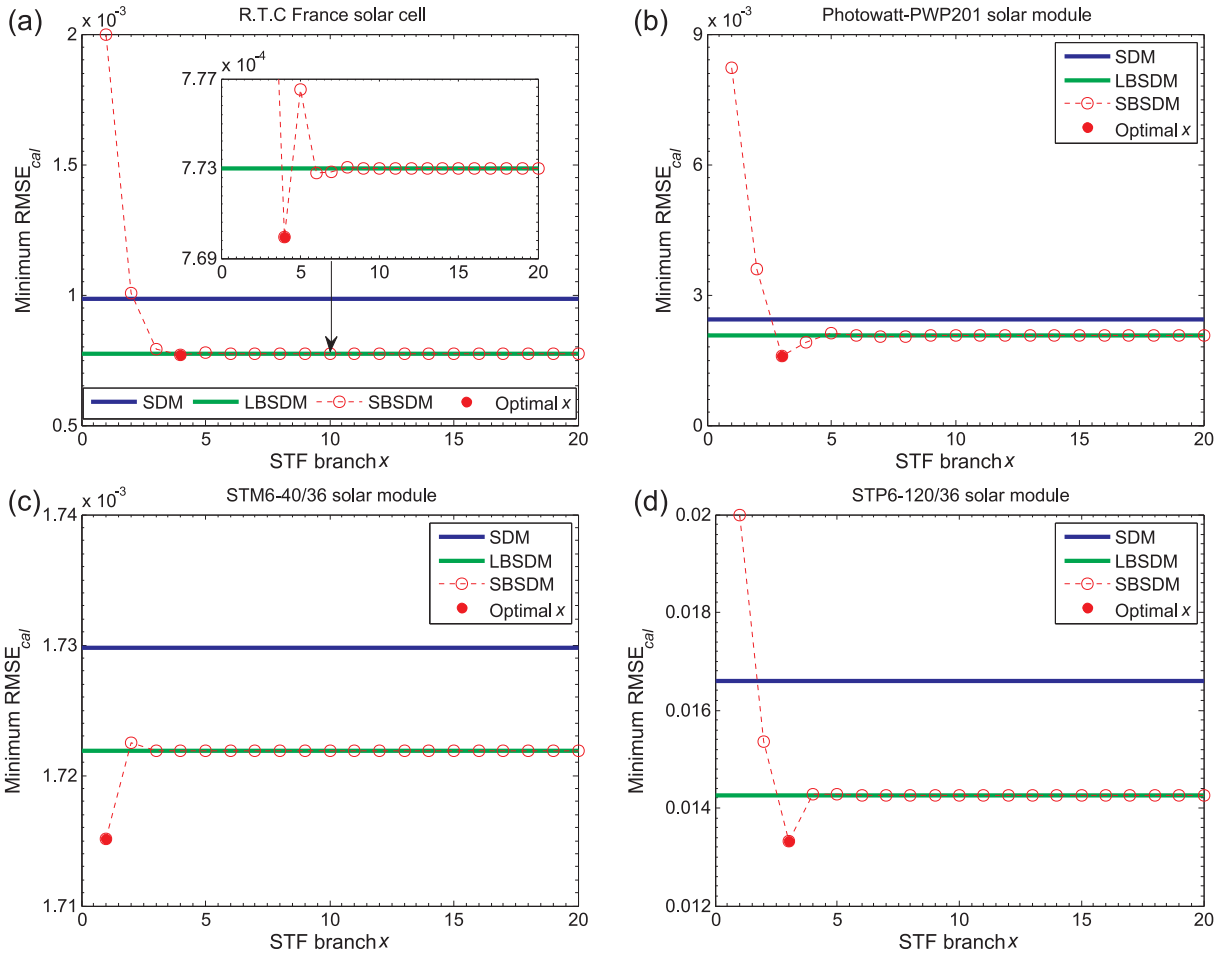

Fig. 12. Minimum $RMSE_{cal}$ values derived from fixed x in parameter extraction of SBSDM of four solar cell/modules. For easy comparison and crosschecking, the minimum $RMSE_{cal}$ values of SDM and LBSDM are also plotted here.

in the knowledge about the real values of solar cell parameters. Furthermore, as can be seen from Tables 7–10 that although the $RMSE_{sim}$ values of LBSDM are smaller than those of SDM, but the sum of ACE_{sim} values of LBSDM of Photowatt-PWP201 and STM6-40/36 modules are bigger than that of SDM. That is to say, there is no guarantee the sum of ACE_{sim} value of LBSDM is always smaller than that of SDM. On the contrary, no such phenomena exist in SBSDM, which endows SBSDM more reliable accuracy than LBSDM.

Table 6
Optimal parameter values and $RMSE_{cal}$ values extracted by MNMS algorithm for SDM, LBSDM and SBSDM of four solar cell/modules.

Models	I_{ph} (A)	I_0 (μA)	n	R_s (Ω)	R_{sh} (Ω)	Optimal x	$RMSE_{cal}$
R.T.C France solar cell [28]							
SDM	0.76077553	0.32302079	1.48118359	0.03637709	53.71852263		9.86021878E−04
LBSDM	0.76078797	0.31068460	1.47726779	0.03654695	52.88978879		7.73006269E−04
SBSDM	0.76078673	0.31319537	1.47801773	0.03645168	52.92130118	4	7.69962109E−04
Photowatt-PWP201 module [28]							
SDM	1.03051430	3.48226272	48.64283465	1.20127101	981.98218515		2.42507487E−03
LBSDM	1.03143382	2.63807707	47.59822391	1.23563416	821.64132603		2.05296064E−03
SBSDM	1.03245776	1.43314631	45.54405352	1.38018865	706.40146172	3	1.59598603E−03
STM6-40/36 module [51]							
SDM	1.66390478	1.73865691	54.73090521	0.15385577	573.41859547		1.72981371E−03
LBSDM	1.66390345	1.74124572	54.73680057	0.15364023	573.53391563		1.72192151E−03
SBSDM	1.66383349	1.83259806	54.89533563	0.13523508	575.57153878	1	1.71516650E−03
STP6-120/36 module [51]							
SDM	7.47252992	2.33499500	45.36372514	0.16540685	799.91629335		1.66006031E−02
LBSDM	7.47528407	1.93088803	44.80042312	0.16891818	570.19743453		1.42510636E−02
SBSDM	7.47795003	1.36073030	43.86106679	0.18073186	442.08938696	3	1.33172872E−02

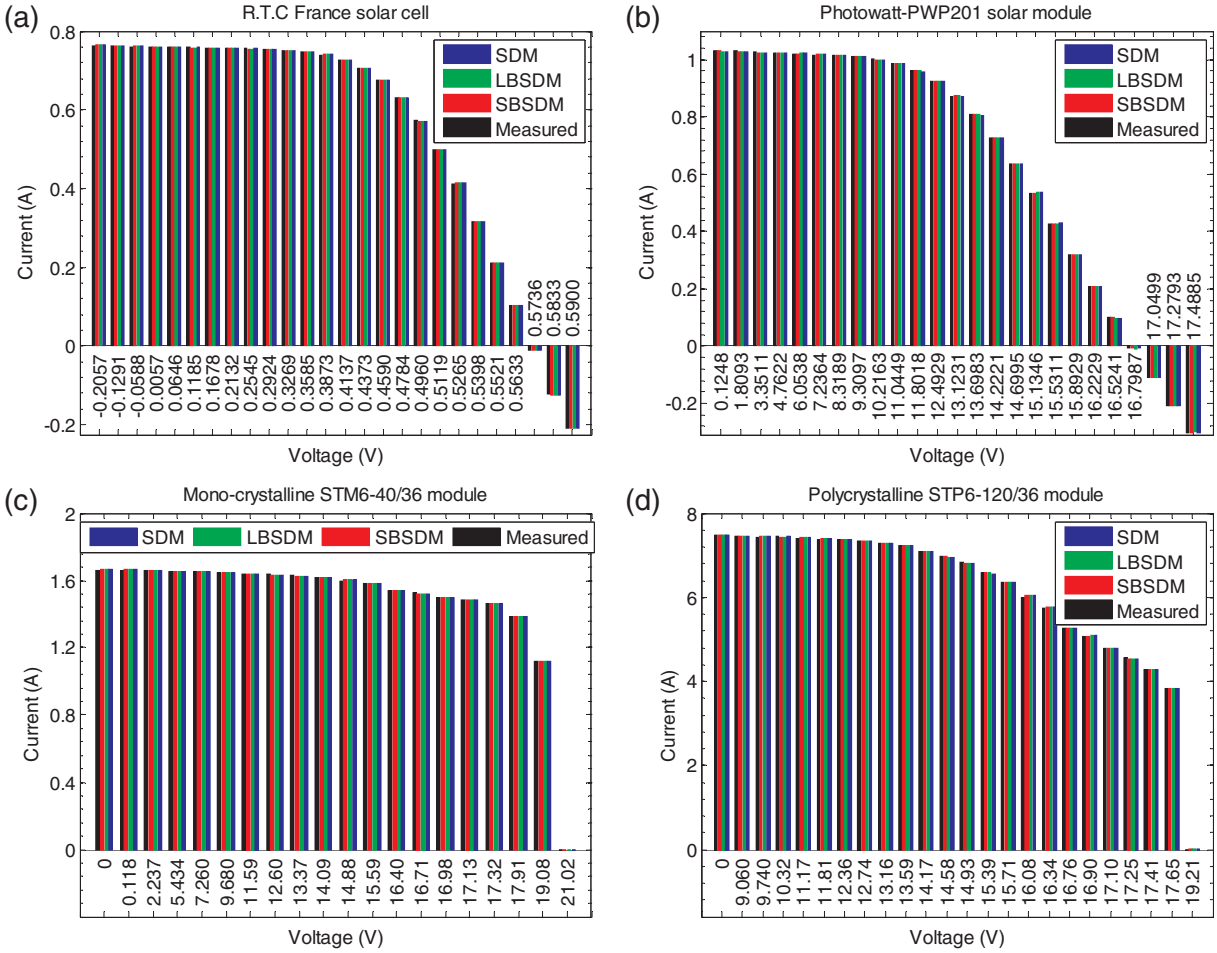

Fig. 13. Simulated *I–V* data of SDM, LBSDM and SBSDM reconstructed using the optimal parameter values extracted by MNMS algorithm and the measured voltage of four solar cell/modules.

6. Conclusion and future research

This paper offers a comprehensive performance comparison of SBSDM, LBSDM and SDM. These three models are closely linked with but different from each other. On the first hand, SBSDM and LBSDM are exactly derived from SDM with the identical model parameters. On the other hand, owing to the difference of exponential function, Lambert *W* function and STF, they are expressed and calculated in different ways and thus have different performance. In this paper, the difference of SBSDM, LBSDM and SDM is demonstrated in two aspects: (1) different fitness to the measured *I–V* data of solar cells, and (2) different parameter extraction performance. The fitness difference of the three models is objectively validated by the reported parameter values of standard datasets and measured datasets. The comparison results indicate that SBSDM always exhibits better fitness than LBSDM and SDM in representing the *I–V* characteristics of various solar cells and can provide a closer prediction to actual MPP. The reason behind this difference is that SDM is an implicit transcendental equation; LBSDM is an exact explicit expression of SDM, while SBSDM is a multi-branched exact explicit expression of SDM. The parameter extraction performance of SBSDM, LBSDM and SDM is compared in commonly used double precision arithmetic using proposed MNMS algorithm and a ranking based STF branch selection strategy. The comparison results reveal that the time computational efficiency of SBSDM is inferior to SDM but superior to LBSDM. Despite lacking enough statistical robustness, SBSDM always acquires superior accuracy and convergence speed than LBSDM and SDM. The reason behind this difference is that the exact explicit multi-branch of SBSDM is very much a double-edged sword, increasing the selectivity while decreasing the probability of finding the optimal STF branch to extract the most accurate parameter values.

All above results provide sufficient evidences that SBSDM is quite promising and envisaged to be the most valuable model for solar cell simulation. Given the significant superiority of SBSDM, two interesting directions are suggested for future research. Since the ranking-based selection strategy proposed in this paper is not good enough to obtain the optimal STF branch for parameter extraction of SBSDM, the reader is encouraged to use some swarm intelligence algorithms to improve its reliability and stability, which will endow a better understanding of the parameters that affect cell performance. The other direction is to extend

Table 7
Simulated current data and absolute current errors of SDM, LBSDM and SBSDM reconstructed using the measured voltage of R.T.C France solar cell [28] and the optimal parameter values extracted by MNMS algorithm.

Item	Measured data		SDM		LBSDM		SBSDM	
	V (V)	I (A)	I_{sim} (A)	ACE_{sim} (A)	I_{sim} (A)	ACE_{sim} (A)	I_{sim} (A)	ACE_{sim} (A)
1	−0.2057	0.7640	0.76408764	0.00008764	0.76414946	0.00014946	0.76414761	0.00014761
2	−0.1291	0.7620	0.76266264	0.00066264	0.76270215	0.00070215	0.76270115	0.00070115
3	−0.0588	0.7605	0.76135473	0.00085473	0.76137377	0.00087377	0.76137356	0.00087356
4	0.0057	0.7605	0.76015423	0.00034577	0.76015450	0.00034550	0.76015501	0.00034499
5	0.0646	0.7600	0.75905585	0.00094415	0.75903905	0.00096095	0.75904021	0.00095979
6	0.1185	0.7590	0.75804301	0.00095699	0.75801075	0.00098925	0.75801247	0.00098753
7	0.1678	0.7570	0.75709159	0.00009159	0.75704570	0.00004570	0.75704785	0.00004785
8	0.2132	0.7570	0.75614207	0.00085793	0.75608482	0.00091518	0.75608720	0.00091280
9	0.2545	0.7555	0.75508732	0.00041268	0.75502235	0.00047765	0.75502455	0.00047545
10	0.2924	0.7540	0.75366447	0.00033553	0.75359735	0.00040265	0.75359874	0.00040126
11	0.3269	0.7505	0.75138806	0.00088806	0.75132726	0.00082726	0.75132695	0.00082695
12	0.3585	0.7465	0.74734834	0.00084834	0.74730534	0.00080534	0.74730238	0.00080238
13	0.3873	0.7385	0.74009688	0.00159688	0.74008463	0.00158463	0.74007858	0.00157858
14	0.4137	0.7280	0.72739678	0.00060322	0.72742619	0.00057381	0.72741791	0.00058209
15	0.4373	0.7065	0.70695327	0.00045327	0.70702593	0.00052593	0.70701837	0.00051837
16	0.4590	0.6755	0.67529489	0.00020511	0.67540033	0.00009967	0.67539816	0.00010184
17	0.4784	0.6320	0.63088431	0.00111569	0.63099815	0.00100185	0.63100543	0.00099457
18	0.4960	0.5730	0.57208207	0.00091793	0.57217471	0.00082529	0.57219156	0.00080844
19	0.5119	0.4990	0.49949164	0.00049164	0.49953898	0.00053898	0.49955878	0.00055878
20	0.5265	0.4130	0.41349356	0.00049356	0.41348487	0.00048487	0.41349502	0.00049502
21	0.5398	0.3165	0.31721950	0.00071950	0.31716154	0.00066154	0.31715050	0.00065050
22	0.5521	0.2120	0.21210317	0.00010317	0.21201673	0.00001673	0.21198620	0.00001380
23	0.5633	0.1035	0.10272135	0.00077865	0.10263674	0.00086326	0.10261018	0.00088982
24	0.5736	−0.0100	−0.00924885	0.00075115	−0.00929831	0.00070169	−0.00929011	0.00070989
25	0.5833	−0.1230	−0.12438136	0.00138136	−0.12436133	0.00136133	−0.12432521	0.00132521
26	0.5900	−0.2100	−0.20919308	0.00080692	−0.20910168	0.00089832	−0.20911306	0.00088694
Sum of ACE_{sim}	—	—	—	0.01770412	—	0.01763274	—	0.01759515
$RMSE_{sim}$	—	—	—	7.75391248E−04	—	7.73006269E−04	—	7.69962109E−04

Table 8
Simulated current data and absolute current errors of SDM, LBSDM and SBSDM reconstructed using the measured voltage of Photowatt- PWP201 module [28] and the optimal parameter values extracted by MNMS algorithm.

Item	Measured data		SDM		LBSDM		SBSDM	
	V (V)	I (A)	I_{sim} (A)	ACE_{sim} (A)	I_{sim} (A)	ACE_{sim} (A)	I_{sim} (A)	ACE_{sim} (A)
1	0.1248	1.0315	1.02912209	0.00237791	1.02972830	0.00177170	1.03026462	0.00123538
2	1.8093	1.0300	1.02738435	0.00261565	1.02766102	0.00233898	1.02787061	0.00212939
3	3.3511	1.0260	1.02574214	0.00025786	1.02572451	0.00027549	1.02564616	0.00035384
4	4.7622	1.0220	1.02410399	0.00210399	1.02383338	0.00183338	1.02351656	0.00151656
5	6.0538	1.0180	1.02228341	0.00428341	1.02181372	0.00381372	1.02132861	0.00332861
6	7.2364	1.0155	1.01991740	0.00441740	1.01932308	0.00382308	1.01877163	0.00327163
7	8.3189	1.0140	1.01635081	0.00235081	1.01573338	0.00173338	1.01525486	0.00125486
8	9.3097	1.0100	1.01049143	0.00049143	1.00997866	0.00002134	1.00973790	0.00026210
9	10.2163	1.0035	1.00067876	0.00282124	1.00040950	0.00309050	1.00055435	0.00294565
10	11.0449	0.9880	0.98465335	0.00334665	0.98474272	0.00325728	0.98532734	0.00267266
11	11.8018	0.9630	0.95969741	0.00330259	0.96018869	0.00281131	0.96109127	0.00190873
12	12.4929	0.9255	0.92304875	0.00245125	0.92387377	0.00162623	0.92477391	0.00072609
13	13.1231	0.8725	0.87258816	0.00008816	0.87356671	0.00106671	0.87404888	0.00154888
14	13.6983	0.8075	0.80731012	0.00018988	0.80820315	0.00070315	0.80797034	0.00047034
15	14.2221	0.7265	0.72795782	0.00145782	0.72855016	0.00205016	0.72762682	0.00112682
16	14.6995	0.6345	0.63646618	0.00196618	0.63663357	0.00213357	0.63540114	0.00090114
17	15.1346	0.5345	0.53569607	0.00119607	0.53542821	0.00092821	0.53445116	0.00004884
18	15.5311	0.4275	0.42881615	0.00131615	0.42819954	0.00069954	0.42793327	0.00043327
19	15.8929	0.3185	0.31866866	0.00016866	0.31785011	0.00064989	0.31840822	0.00009178
20	16.2229	0.2085	0.20785711	0.00064289	0.20700827	0.00149173	0.20811580	0.00038420
21	16.5241	0.1010	0.09835421	0.00264579	0.09764456	0.00335544	0.09878812	0.00221188
22	16.7987	−0.0080	−0.00816934	0.00016934	−0.00858898	0.00058898	−0.00791181	0.00008819
23	17.0499	−0.1110	−0.11096846	0.00003154	−0.11097201	0.00002799	−0.11102409	0.00002409
24	17.2793	−0.2090	−0.20911762	0.00011762	−0.20860706	0.00039294	−0.20927032	0.00027032
25	17.4885	−0.3030	−0.30202238	0.00097762	−0.30092697	0.00207303	−0.30167536	0.00132464
Sum of ACE_{sim}	—	—	—	0.04178790	—	0.04255774	—	0.03052989
$RMSE_{sim}$	—	—	—	2.13852591E−03	—	2.05296064E−03	—	1.59598603E−03

Table 9
Simulated current data and absolute current errors of SDM, LBSDM and SBSDM reconstructed using the measured voltage of STM6-40/36 module [51] and the optimal parameter values extracted by MNMS algorithm.

Item	Measured data		SDM		LBSDM		SBSDM	
	V (V)	I (A)	I_{sim} (A)	ACE_{sim} (A)	I_{sim} (A)	ACE_{sim} (A)	I_{sim} (A)	ACE_{sim} (A)
1	0	1.663	1.66345813	0.00045813	1.66345752	0.00045752	1.66344236	0.00044236
2	0.118	1.663	1.66325224	0.00025224	1.66325167	0.00025167	1.66323722	0.00023722
3	2.237	1.661	1.65955120	0.00144880	1.65955136	0.00144864	1.65954970	0.00145030
4	5.434	1.653	1.65391444	0.00091444	1.65391567	0.00091567	1.65393231	0.00093231
5	7.260	1.650	1.65056575	0.00056575	1.65056750	0.00056750	1.65059269	0.00059269
6	9.680	1.645	1.64543044	0.00043044	1.64543257	0.00043257	1.64546196	0.00046196
7	11.59	1.640	1.63923405	0.00076595	1.63923579	0.00076421	1.63925469	0.00074531
8	12.60	1.636	1.63371510	0.00228490	1.63371615	0.00228385	1.63372120	0.00227880
9	13.37	1.629	1.62728848	0.00171152	1.62728869	0.00171131	1.62727911	0.00172089
10	14.09	1.619	1.61831518	0.00068482	1.61831435	0.00068565	1.61828934	0.00071066
11	14.88	1.597	1.60306738	0.00606738	1.60306520	0.00606520	1.60302558	0.00602558
12	15.59	1.581	1.58158500	0.00058500	1.58158166	0.00058166	1.58153800	0.00053800
13	16.40	1.542	1.54232745	0.00032745	1.54232347	0.00032347	1.54229803	0.00029803
14	16.71	1.524	1.52122497	0.00277503	1.52122119	0.00277881	1.52121171	0.00278829
15	16.98	1.500	1.49920572	0.00079428	1.49920241	0.00079759	1.49921106	0.00078894
16	17.13	1.485	1.48527115	0.00027115	1.48526826	0.00026826	1.48528843	0.00028843
17	17.32	1.465	1.46564321	0.00064321	1.46564105	0.00064105	1.46567687	0.00067687
18	17.91	1.388	1.38759934	0.00040066	1.38760106	0.00039894	1.38768295	0.00031705
19	19.08	1.118	1.11837210	0.00037210	1.11839036	0.00039036	1.11832664	0.00032664
20	21.02	0	−0.00002131	0.00002131	−0.00002593	0.00002593	−0.00001987	0.00001987
Sum of ACE_{sim}	—	—	—	0.02177457	—	0.02178986	—	0.02164020
$RMSE_{sim}$	—	—	—	1.72192793E−03	—	1.72192151E−03	—	1.71516650E−03

Table 10
Simulated current data and absolute current errors of SDM, LBSDM and SBSDM reconstructed using the measured voltage of STP6-120/36 module [51] and the optimal parameter values extracted by MNMS algorithm.

Item	Measured data		SDM		LBSDM		SBSDM	
	V (V)	I (A)	I_{sim} (A)	ACE_{sim} (A)	I_{sim} (A)	ACE_{sim} (A)	I_{sim} (A)	ACE_{sim} (A)
1	0	7.48	7.47098128	0.00901872	7.47306692	0.00693308	7.47489152	0.00510848
2	9.06	7.45	7.45253755	0.00253755	7.45053567	0.00053567	7.44842129	0.00157871
3	9.74	7.42	7.44671497	0.02671497	7.44462650	0.02462650	7.44251927	0.02251927
4	10.32	7.44	7.43909223	0.00090777	7.43702665	0.00297335	7.43505295	0.00494705
5	11.17	7.41	7.42026500	0.01026500	7.41845948	0.00845948	7.41696622	0.00696622
6	11.81	7.38	7.39587314	0.01587314	7.39449833	0.01449833	7.39363985	0.01363985
7	12.36	7.37	7.36326479	0.00673521	7.36245545	0.00754455	7.36233932	0.00766068
8	12.74	7.34	7.33148307	0.00851693	7.33117566	0.00882434	7.33166057	0.00833943
9	13.16	7.29	7.28412985	0.00587015	7.28447463	0.00552537	7.28566581	0.00433419
10	13.59	7.23	7.21776060	0.01223940	7.21885100	0.01114900	7.22073460	0.00926540
11	14.17	7.10	7.08813731	0.01186269	7.09025066	0.00974934	7.09279786	0.00720214
12	14.58	6.97	6.95844905	0.01155095	6.96117548	0.00882452	6.96380543	0.00619457
13	14.93	6.83	6.81486011	0.01513989	6.81793405	0.01206595	6.82025540	0.00974460
14	15.39	6.58	6.56792937	0.01207063	6.57106080	0.00893920	6.57235634	0.00764366
15	15.71	6.36	6.34872742	0.01127258	6.35154515	0.00845485	6.35175683	0.00824317
16	16.08	6.00	6.03749239	0.03749239	6.03953299	0.03953299	6.03833182	0.03833182
17	16.34	5.75	5.77681380	0.02681380	5.77804846	0.02804846	5.77598030	0.02598030
18	16.76	5.27	5.27376516	0.00376516	5.27334588	0.00334588	5.27074538	0.00074538
19	16.9	5.07	5.08193389	0.01193389	5.08090715	0.01090715	5.07853012	0.00853012
20	17.1	4.79	4.78583302	0.00416698	4.78393508	0.00606492	4.78234865	0.00765135
21	17.25	4.56	4.54628941	0.01371059	4.54376299	0.01623701	4.54317730	0.01682270
22	17.41	4.29	4.27392907	0.01607093	4.27078564	0.01921436	4.27167068	0.01832932
23	17.65	3.83	3.83228232	0.00228232	3.82838370	0.00161630	3.83220186	0.00220186
24	19.21	0	0.00116435	0.00116435	0.00416170	0.00416170	0.00415065	0.00415065
Sum of ACE_{sim}	—	—	—	0.27797598	—	0.26823230	—	0.24613092
$RMSE_{sim}$	—	—	—	1.44183789E−02	—	1.42510636E−02	—	1.33172872E−02

the application of SBSDM in energy yield calculations and maximum energy harvesting of PV systems.

Acknowledgments

The authors are thankful to the responsible editor and the anonymous reviewers for their valuable comments and insightful suggestions. The authors gratefully acknowledge the PV Performance Modeling Collaborative group at Sandia National Laboratories for their kindly providing the source codes of pvl_lambertw.m. This work was financially supported by the Plan for Scientific Innovation Talent of Henan Province [grant number 174100510020], Henan Province Institution of Higher Learning Youth Backbone Teachers Training Program [grant number 2016GGJS-0360], the Program for Science & Technology Innovation Talents in Universities of Henan Province [grant number 16HASTIT026] and the National Natural Science Foundation of China [grant number 51576060].

References

[1] Et-torabi K, Nassar-eddine I, Obbadi A, Errami Y, Rmaily R, Sahnoun S, et al. Parameters estimation of the single and double diode photovoltaic models using a Gauss-Seidel algorithm and analytical method: A comparative study. Energy Convers Manage 2017;148:1041–54. http://dx.doi.org/10.1016/j.enconman.2017.06.064.

[2] Femia N, Petrone G, Spagnuolo G, Vitelli M. Power electronics and control techniques for maximum energy harvesting in photovoltaic systems. CRC Press; 2012.

[3] Chin VJ, Salam Z, Ishaque K. Cell modelling and model parameters estimation techniques for photovoltaic simulator application: A review. Appl Energy 2015;154:500–19. http://dx.doi.org/10.1016/j.apenergy.2015.05.035.

[4] Gao X, Cui Y, Hu J, Xu G, Wang Z, Qu J, et al. Parameter extraction of solar cell models using improved shuffled complex evolution algorithm. Energy Convers Manage 2018;157:460–79. http://dx.doi.org/10.1016/j.enconman.2017.12.033.

[5] Chen Z, Wu L, Lin P, Wu Y, Cheng S. Parameters identification of photovoltaic models using hybrid adaptive Nelder-Mead simplex algorithm based on eagle strategy. Appl Energy 2016;182:47–57. http://dx.doi.org/10.1016/j.apenergy.2016.08.083.

[6] Nassar-eddine I, Obbadi A, Errami Y, El fajri A, Agunaou M. Parameter estimation of photovoltaic modules using iterative method and the Lambert W function: A comparative study. Energy Convers Manage 2016;119:37–48. http://dx.doi.org/10.1016/j.enconman.2016.04.030.

[7] Batzelis EI, Kampitsis GE, Papathanassiou SA, Manias SN. Direct MPP calculation in terms of the single-diode PV model parameters. IEEE Trans Energy Convers 2015;30:226–36. http://dx.doi.org/10.1109/TEC.2014.2356017.

[8] Dileep G, Singh SN. Application of soft computing techniques for maximum power point tracking of SPV system. Sol Energy 2017;141:182–202. http://dx.doi.org/10.1016/j.solener.2016.11.034.

[9] Kheldoun A, Bradai R, Boukenoui R, Mellit A. A new Golden Section method-based maximum power point tracking algorithm for photovoltaic systems. Energy Convers Manage 2016;111:125–36. http://dx.doi.org/10.1016/j.enconman.2015.12.039.

[10] Chen Z, Wu L, Cheng S, Lin P, Wu Y, Lin W. Intelligent fault diagnosis of photovoltaic arrays based on optimized kernel extreme learning machine and I-V characteristics. Appl Energy 2017;204:912–31. http://dx.doi.org/10.1016/j.apenergy.2017.05.034.

[11] Lin P, Cheng S, Yeh W, Chen Z, Wu L. Parameters extraction of solar cell models using a modified simplified swarm optimization algorithm. Sol Energy 2017;144:594–603. http://dx.doi.org/10.1016/j.solener.2017.01.064.

[12] Nunes HGG, Pombo JAN, Mariano SJPS, Calado MRA, Felippe de Souza JAM. A new high performance method for determining the parameters of PV cells and modules based on guaranteed convergence particle swarm optimization. Appl Energy 2018;211:774–91. http://dx.doi.org/10.1016/j.apenergy.2017.11.078.

[13] Jain A, Kapoor A. Exact analytical solutions of the parameters of real solar cells using Lambert W-function. Sol Energy Mater Sol Cells 2004;81:269–77. http://dx.doi.org/10.1016/j.solmat.2003.11.018.

[14] Veberič D. Lambert W function for applications in physics. Comput Phys Commun 2012;183:2622–8. http://dx.doi.org/10.1016/j.cpc.2012.07.008.

[15] Gao X, Cui Y, Hu J, Xu G, Yu Y. Lambert W-function based exact representation for double diode model of solar cells: Comparison on fitness and parameter extraction. Energy Convers Manage 2016;127:443–60. http://dx.doi.org/10.1016/j.enconman.2016.09.005.

[16] Fukushima T. Precise and fast computation of Lambert W-functions without transcendental function evaluations. J Comput Appl Math 2013;244:77–89. http://dx.doi.org/10.1016/j.cam.2012.11.021.

[17] Li Y, Huang W, Huang H, Hewitt C, Chen Y, Fang G, et al. Evaluation of methods to extract parameters from current–voltage characteristics of solar cells. Sol Energy 2013;90:51–7. http://dx.doi.org/10.1016/j.solener.2012.12.005.

[18] Perovich SM, Bauk SI, Jovanovic MD. Concerning an analytical solution of some families of nonlinear functional equations. AIP Conf Proc 2007;936:412–5. http://dx.doi.org/10.1063/1.2790165.

[19] Santakrus Singh N, Jain A, Kapoor A. Determination of the solar cell junction ideality factor using special trans function theory (STFT). Sol Energy Mater Sol Cells 2009;93:1423–6. http://dx.doi.org/10.1016/j.solmat.2009.03.013.

[20] Perovich SM, Calasan MP. Obtaining an analytical STFT closed form solution to the solar cell junction ideality factor using the maximum power point characteristics. In: 2014 IEEE international energy conference (ENERGYCON); 2014. p. 922–8. http://dx.doi.org/10.1109/ENERGYCON.2014.6850536.

[21] Perovich SM, Djukanovic MD, Dlabac T, Nikolic D, Calasan MP. Concerning a novel mathematical approach to the solar cell junction ideality factor estimation. Appl Math Model 2015;39:3248–64. http://dx.doi.org/10.1016/j.apm.2014.11.026.

[22] Singh NS, Jain A, Kapoor A. A new method to determine the optimum load of a real solar cell using special trans function theory (STFT). Int J Renew Energy Res 2013;3:378–82http://www.ijrer.org/ijrer/index.php/ijrer/article/view/611/pdf.

[23] Singh NS, Jain A, Kapoor A. An exact analytical method for calculating the parameters of a real solar cell using special trans function theory (STFT). Int J Renew Energy Res 2013;3:202–6http://www.ijrer.org/ijrer/index.php/ijrer/article/view/549/pdf.

[24] Singh NS, Jain A, Kapoor A. Exact analytical solution for organic solar cells showing S-shaped J-V characteristics using special trans function theory (STFT). Int J Renew Energy Res 2013;3http://www.ijrer.org/ijrer/index.php/ijrer/article/view/719/pdf.

[25] Askarzadeh A, dos Santos Coelho L. Determination of photovoltaic modules parameters at different operating conditions using a novel bird mating optimizer approach. Energy Convers Manage 2015;89:608–14. http://dx.doi.org/10.1016/j.enconman.2014.10.025.

[26] Jiang LL, Maskell DL, Patra JC. Parameter estimation of solar cells and modules using an improved adaptive differential evolution algorithm. Appl Energy 2013;112:185–93. http://dx.doi.org/10.1016/j.apenergy.2013.06.004.

[27] Ishaque K, Salam Z, Mekhilef S, Shamsudin A. Parameter extraction of solar photovoltaic modules using penalty-based differential evolution. Appl Energy 2012;99:297–308. http://dx.doi.org/10.1016/j.apenergy.2012.05.017.

[28] Easwarakhanthan T, Bottin J, Bouhouch I, Boutrit C. Nonlinear minimization algorithm for determining the solar cell parameters with microcomputers. Int J Sol Energy 1986;4:1–12. http://dx.doi.org/10.1080/01425918608909835.

[29] Gong W, Cai Z. Parameter extraction of solar cell models using repaired adaptive differential evolution. Sol Energy 2013;94:209–20. http://dx.doi.org/10.1016/j.solener.2013.05.007.

[30] Kler D, Sharma P, Banerjee A, Rana KPS, Kumar V. PV cell and module efficient parameters estimation using evaporation rate based water cycle algorithm. Swarm Evol Comput 2017. http://dx.doi.org/10.1016/j.swevo.2017.02.005.

[31] Guo L, Meng Z, Sun Y, Wang L. Parameter identification and sensitivity analysis of solar cell models with cat swarm optimization algorithm. Energy Convers Manage 2016;108:520–8. http://dx.doi.org/10.1016/j.enconman.2015.11.041.

[32] Hamid NFA, Rahim NA, Selvaraj J. Solar cell parameters identification using hybrid Nelder-Mead and modified particle swarm optimization. J Renew Sustain Energy 2016;8. http://dx.doi.org/10.1063/1.4941791.

[33] Askarzadeh A, Rezazadeh A. Extraction of maximum power point in solar cells using bird mating optimizer-based parameters identification approach. Sol Energy 2013;90:123–33. http://dx.doi.org/10.1016/j.solener.2013.01.010.

[34] Dkhichi F, Oukarfi B, Fakkar A, Belbounaguia N. Parameter identification of solar cell model using Levenberg–Marquardt algorithm combined with simulated annealing. Sol Energy 2014;110:781–8. http://dx.doi.org/10.1016/j.solener.2014.09.033.

[35] Niu Q, Zhang L, Li K. A biogeography-based optimization algorithm with mutation strategies for model parameter estimation of solar and fuel cells. Energy Convers Manage 2014;86:1173–85. http://dx.doi.org/10.1016/j.enconman.2014.06.026.

[36] Chen X, Yu K, Du W, Zhao W, Liu G. Parameters identification of solar cell models using generalized oppositional teaching learning based optimization. Energy 2016;99:170–80. http://dx.doi.org/10.1016/j.energy.2016.01.052.

[37] Askarzadeh A, Rezazadeh A. Parameter identification for solar cell models using harmony search-based algorithms. Sol Energy 2012;86:3241–9. http://dx.doi.org/10.1016/j.solener.2012.08.018.

[38] Askarzadeh A, Rezazadeh A. Artificial bee swarm optimization algorithm for parameters identification of solar cell models. Appl Energy 2013;102:943–9. http://dx.doi.org/10.1016/j.apenergy.2012.09.052.

[39] Ma J, Ting TO, Man KL, Zhang N, Guan S-U, Wong PWH. Parameter estimation of photovoltaic models via cuckoo search. J Appl Math 2013;2013:1–8. http://dx.doi.org/10.1155/2013/362619.

[40] Ma J, Man KL, Guan SU, Ting TO, Wong PWH. Parameter estimation of photovoltaic model via parallel particle swarm optimization algorithm. Int J Energy Res 2016;40:343–52. http://dx.doi.org/10.1002/er.3359.

[41] Niu Q, Zhang H, Li K. An improved TLBO with elite strategy for parameters identification of PEM fuel cell and solar cell models. Int J Hydrogen Energy 2014;39:3837–54. http://dx.doi.org/10.1016/j.ijhydene.2013.12.110.

[42] Zhang Y, Lin P, Chen Z, Cheng S. A population classification evolution algorithm for the parameter extraction of solar cell models. Int J Photoenergy 2016;2016:1–16. http://dx.doi.org/10.1155/2016/2174573.

[43] Oliva D, Cuevas E, Pajares G. Parameter identification of solar cells using artificial bee colony optimization. Energy 2014;72:93–102. http://dx.doi.org/10.1016/j.energy.2014.05.011.

[44] Laudani A, Riganti Fulginei F, Salvini A. High performing extraction procedure for the one-diode model of a photovoltaic panel from experimental I-V curves by using reduced forms. Sol Energy 2014;103:316–26. http://dx.doi.org/10.1016/j.solener.2014.02.014.

[45] Alam DF, Yousri DA, Eteiba MB. Flower pollination algorithm based solar PV parameter estimation. Energy Convers Manage 2015;101:410–22. http://dx.doi.org/10.1016/j.enconman.2015.05.074.

[46] Ram JP, Babu TS, Dragicevic T, Rajasekar N. A new hybrid bee pollinator flower pollination algorithm for solar PV parameter estimation. Energy Convers Manage 2017;135:463–76. http://dx.doi.org/10.1016/j.enconman.2016.12.082.
[47] Lim LHI, Ye Z, Ye J, Yang D, Du H. A linear identification of diode models from single I-V characteristics of PV panels. IEEE Trans Ind Electron 2015;62:4181–93. http://dx.doi.org/10.1109/TIE.2015.2390193.
[48] Huang W, Jiang C, Xue L, Song D. Extracting solar cell model parameters based on chaos particle swarm algorithm. In: 2011 International conference on electric information and control engineering; 2011. p. 398–402. http://dx.doi.org/10.1109/ICEICE.2011.5777246.
[49] Yuan X, Xiang Y, He Y. Parameter extraction of solar cell models using mutative-scale parallel chaos optimization algorithm. Sol Energy 2014;108:238–51. http://dx.doi.org/10.1016/j.solener.2014.07.013.
[50] Hachana O, Hemsas KE, Tina GM, Ventura C. Comparison of different metaheuristic algorithms for parameter identification of photovoltaic cell/module. J Renew Sustain Energy 2013;5:053122http://dx.doi.org/10.1063/1.4822054.
[51] Tong NT, Pora W. A parameter extraction technique exploiting intrinsic properties of solar cells. Appl Energy 2016;176:104–15. http://dx.doi.org/10.1016/j.apenergy.2016.05.064.
[52] Jamadi M, Merrikh-Bayat F, Bigdeli M. Very accurate parameter estimation of single- and double-diode solar cell models using a modified artificial bee colony algorithm. Int J Energy Environ Eng 2016;7:13–25. http://dx.doi.org/10.1007/s40095-015-0198-5.
[53] Jordehi AR. Time varying acceleration coefficients particle swarm optimisation (TVACPSO): A new optimisation algorithm for estimating parameters of PV cells and modules. Energy Convers Manage 2016;129:262–74. http://dx.doi.org/10.1016/j.enconman.2016.09.085.
[54] Yuan X, He Y, Liu L. Parameter extraction of solar cell models using chaotic asexual reproduction optimization. Neural Comput Appl 2015;26:1227–39. http://dx.doi.org/10.1007/s00521-014-1795-6.
[55] Ye M, Wang X, Xu Y. Parameter extraction of solar cells using particle swarm optimization. J Appl Phys 2009;105:1–8. http://dx.doi.org/10.1063/1.3122082.
[56] Patel SJ, Panchal AK, Kheraj V. Extraction of solar cell parameters from a single current–voltage characteristic using teaching learning based optimization algorithm. Appl Energy 2014;119:384–93. http://dx.doi.org/10.1016/j.apenergy.2014.01.027.
[57] AlHajri MF, El-Naggar KM, AlRashidi MR, Al-Othman AK. Optimal extraction of solar cell parameters using pattern search. Renew Energy 2012;44:238–45. http://dx.doi.org/10.1016/j.renene.2012.01.082.
[58] El-Naggar KM, AlRashidi MR, AlHajri MF, Al-Othman AK. Simulated annealing algorithm for photovoltaic parameters identification. Sol Energy 2012;86:266–74. http://dx.doi.org/10.1016/j.solener.2011.09.032.
[59] AlRashidi MR, AlHajri MF, El-Naggar KM, Al-Othman AK. A new estimation approach for determining the I-V characteristics of solar cells. Sol Energy 2011;85:1543–50. http://dx.doi.org/10.1016/j.solener.2011.04.013.
[60] Chellaswamy C, Ramesh R. Parameter extraction of solar cell models based on adaptive differential evolution algorithm. Renew Energy 2016;97:823–37. http://dx.doi.org/10.1016/j.renene.2016.06.024.
[61] Fathy A, Rezk H. Parameter estimation of photovoltaic system using imperialist competitive algorithm. Renew Energy 2017;111:307–20. http://dx.doi.org/10.1016/j.renene.2017.04.014.
[62] El-Fergany A. Efficient tool to characterize photovoltaic generating systems using mine blast algorithm. Electr Power Compon Syst 2015;43:890–901. http://dx.doi.org/10.1080/15325008.2015.1014579.
[63] Ali EE, El-Hameed MA, El-Fergany AA, El-Arini MM. Parameter extraction of photovoltaic generating units using multi-verse optimizer. Sustain Energy Technol Assess 2016;17:68–76http://dx.doi.org//10.1016/j.seta.2016.08.004.
[64] Nelder-Mead algorithm. http://www.scholarpedia.org/article/Nelder-Mead_algorithm.
[65] Press WH, Teukolsky SA, Vetterling WT, Flannery BP. Numerical recipes: The art of scientific computing. 3rd ed. New York: Cambridge University Press; 2007.
[66] Gao F, Han L. Implementing the Nelder-Mead simplex algorithm with adaptive parameters. Comput Optim Appl 2012;51:259–77. http://dx.doi.org/10.1007/s10589-010-9329-3.
[67] Bound constrained optimization using fminsearch. http://www.mathworks.cn/matlabcentral/fileexchange/8277-fminsearchbnd-fminsearchcon.
[68] Mallard T. An improved Nelder-Mead method for analog design optimisation applied to deep sub-micron technology. In: 2014 25th IET Irish signals & systems conference; 2014. p. 164–8. http://dx.doi.org/10.1049/cp.2014.0678.
[69] pvl_lambertw.m. https://pvpmc.sandia.gov/PVLIB_Matlab_Help/html/pvl_lambertw_help.html.